ISSN 1580-4003

THE SCIENTIFIC JOURNAL OF THE VETERINARY FACULTY UNIVERSITY OF LJUBLJANA

SLOVENIAN VETERINARY RESEARCH

SLOVENSKI VETERINARSKI ZBORNIK

Slov Vet Res 2021; 58 (4): 121–160

Volume 58 4

Slov Vet Res • Ljubljana • 2021 • Volume 58 • Number 4 • 121–160

THE SCIENTIFIC JOURNAL OF THE VETERINARY FACULTY UNIVERSITY OF LJUBLJANA

SLOVENIAN VETERINARY RESEARCH

SLOVENSKI VETERINARSKI ZBORNIK

Volume 58 4

Slov Vet Res • Ljubljana • 2021 • Volume 58 • Number 4 • 121–160

The Scientific Journal of the Veterinary Faculty University of Ljubljana

SLOVENIAN VETERINARY RESEARCH
SLOVENSKI VETERINARSKI ZBORNIK

Previously: RESEARCH REPORTS OF THE VETERINARY FACULTY UNIVERSITY OF LJUBLJANA
Prej: ZBORNIK VETERINARSKE FAKULTETE UNIVERZA V LJUBLJANI

4 issues per year / izhaja štirikrat letno
Volume 58, Number 4 / Letnik 58, Številka 4

Editor in Chief / glavna in odgovorna urednica: Klementina Fon Tacer
Co-Editor / sourednik: Modest Vengušt
Technical Editor / tehnični urednik: Matjaž Uršič
Assistant to Editor / pomočnica urednice: Valentina Kubale Dvojmoč

Published by / Založila: University of Ljubljana Press / Založba Univerze v Ljubljani
For the Publisher / Za založbo: Majdič Gregor, the Rector of the University of Ljubljana / rektor Univerze v Ljubljani

Issued by / Izdala: Veterinary Faculty University of Ljubljana / Veterinarska fakulteta Univerze v Ljubljani
For the Issuer / Za izdajatelja: Breda Jakovac Strain, the Dean of the Veterinary Faculty / dekanja Veterinarske fakultete

Address: Veterinary Faculty, Gerbičeva 60, 1000 Ljubljana, Slovenia
Naslov: Veterinarska fakulteta, Gerbičeva 60, 1000 Ljubljana, Slovenija
Tel.: +386 (0)1 47 79 100, Fax: +386 (0)1 28 32 243
E-mail: slovetres@vf.uni-lj.si

Sponsored by the Slovenian Research Agency
Sofinancira: Javna agencija za raziskovalno dejavnost Republike Slovenije

ISSN 1580-4003
Printed by/tisk: DZS, d.d., Ljubljana, December 2021
Number of copies printed / Naklada: 220
Indexed in/indeksirano v: Agris, Biomedicina Slovenica, CAB Abstracts, IVSI
Urlich's International Periodicals Directory, Science Citation Index Expanded,
Journal Citation Reports – Science Edition
https://www.slovetres.si/

SLOVENIAN VETERINARY RESEARCH
SLOVENSKI VETERINARSKI ZBORNIK

Slov Vet Res 2021; 58 (4)

Original Research Articles

Case Report

Slov Vet Res 2021: 58 (4): 125 – 36
DOI 10.26873/SVR-1155-2021
UDC 57.086:611.013.1:57.085.4:591.86+591.88:599.323.451

Original Research Article

ISOLATION OF LIVE CELLS FROM DIFFERENT MICE TISSUES UP TO NINE DAYS AFTER DEATH

Metka Voga[1], Ana Pleterski[1], Gregor Majdič[1,2]*

[1]Institute for preclinical sciences, Veterinary faculty, University of Ljubljana, Gerbiceva 60, Ljubljana, [2]Institute for physiology, Medical faculty, University of Maribor, Taborska 8, Maribor, Slovenia

*Corresponding author, Email: gregor.majdic@vf.uni-lj.si

Abstract: Some limited reports suggest that cells can survive in the cadavers for much longer than it was previously thought. In our study we explored how time after death, tissue type (muscle, brain and adipose tissue), storage temperature of cadavers (4 °C or at room temperature) and form of tissue storage (stored as cadavers or tissue pieces in phosphate buffered saline) affect the success of harvesting live cells from mice after death. Cells were isolated from dead tissues and grown in standard conditions. Some cells were used for RNA extraction and RT² Profiler™ PCR Array for cell lineage identification was performed to establish which lineages the cells obtained from post mortem tissues belong to. Results of our study showed that viable cells can be regularly isolated from muscle and brain tissue 3 days post mortem and with difficulty up to 6 days post mortem. Viable cells from brain tissue can be isolated up to 9 days post mortem. No cells were isolated from adipose tissue except immediately after death. In all instances viable cells were isolated only when tissues were stored at 4 °C. Tissue storage did not affect cell isolation. Isolated cells were progenitors from different germ layers. Our results show that live cells could be obtained from mouse cadavers several days after death.

Key words: mouse; cadaver; stem cells; brain; muscle; adipose tissue

Introduction

Biological death is an irreversible cessation of circulatory and respiratory functions or irreversible cessation of all functions of the entire brain, including the brain stem (1). On the basis of biological death organ and tissue procurement can be processed. Cells that have been successfully used in donor transplantation procedures already in the eighties, were harvested very shortly, usually within 1 hour post mortem (2-4). In recent years, however, several studies have shown that viable cells can survive in the cadavers for much longer than it was previously thought. Viable cells were obtained from different mammalian species at different time periods after death. Viable cells were obtained from murine liver up to 27 hours post mortem (5) and from murine inner ear up to 10 days post mortem (6). Neural stem cells from forebrain of one day old rats were obtained up to 6 days after death (7). Silvestre et al. (8) have obtained viable cells from rabbit and pig ears up to 10 days after death. Fibroblast like cells were recovered from refrigerated goat skin up to 41 days post mortem (9) and cattle skin even up to 49 days post mortem (10). Equine tendons yielded viable stem cells up to 72 hours post mortem (11). From human, myogenic cells were isolated up to 17 days post mortem (12). Results of these studies

Received: 19 September 2020
Accepted for publication: 15 August 2021

suggest that viable cells survive in the cadavers in different tissues for longer time periods after death. It appears in general that viable cells survive in the tissues for longer time after death if tissues or cadavers are stored at 4°C and even longer when stored in liquid nitrogen (13). It is not known what is happening with cells after death. Due to the lack of studies in this area, it is not clear whether cells survive in all tissues or perhaps only in certain niches, neither is certain whether cells in the cadavers remain active or perhaps assume some dormant state. The latter was proposed by Latil et al. (12) who showed that stem cells are enriched in post mortem tissue due to cellular quiescence where cells adopt a reversible dormant state and thus possess a selective survival advantage compared with other cell types. A recent study has shown that also transcriptional activity of genes remains active for at least several hours after death. Appearance of new transcripts was shown in zebra fish and mouse cells up to 48 hours after death. Interestingly, the relative amount of gene transcripts declined gradually after death from the time of death in murine liver, while in murine brain samples, the amount of transcripts actually increased during the first hour after death. Total number of transcripts that increased in murine samples was over 500, suggesting that gene transcription also continues after death (14). However, there are no systematic studies examining the effect of time after death and different storage conditions on success of postmortem cell harvesting. The purpose of our study was therefore to establish the effect of different post mortem time points, tissue type, storage temperature and form of tissue storage on the success of harvesting live cells from mice. Finally, we investigated which lineages the cells obtained from post mortem tissues belong to.

Materials and methods

Animals

In all experiments, adult, 4 to 5 months old, male BALB/C mice were used. Only males were used in this study to reduce the number of animals. Mice were bred at Institute for preclinical sciences with water and food ad libitum in standard conditions (12:12 light dark cycle and room temperature 22 °C). All animal experiments were approved by the Administration of the Republic of Slovenia for Food Safety, Veterinary Sector and Plant Protection of the Republic of Slovenia and were carried out according to ethical principles, EU directive (2010/63/EU), and NIH guidelines. Mice were euthanized by CO_2. The death was confirmed by cardiac arrest. After death mice were used in two ways: some mice (n = 9) were dissected. Approximately 150 mm^3 of adipose tissue, muscle tissue (musculus quadriceps) and brain tissue from hippocampus and subventricular zone was obtained. Dissected tissues were placed in 0.01 M PBS either for storage or for cell isolation at time point 0. Other mice (n = 9) were stored as whole cadavers. Whole cadavers and tissue pieces were stored for 3, 6 and 9 days at 4°C and at room temperature (20–22°C). At given time points cadavers were dissected and the same tissues as those stored in PBS (adipose, muscle and brain tissue from hippocampus and subventricular zone) were obtained. Afterwards tissues both from cadavers and those stored in PBS were further processed.

Cell isolation and cell culture

Time point 0 was used for determination of a better method for cell isolation. Tissues at time point 0 were either enzymatically digested or pieces of tissue were placed directly into tissue culture plates as tissue explants. For enzymatic digestion, tissues were dissected with scalpel into very small pieces and then incubated at 37 °C overnight in Dulbecco – modified eagle medium (DMEM, Gibco, USA) containing 0,1% collagenase type II (Sigma - Aldrich, DE). The digested tissue was centrifuged at 240 rcf/min for 4 minutes. Supernatant was discarded. Pellet was resuspended in cell culture medium containing DMEM and 20% Fetal Bovine Serum (FBS, Gibco, USA). Cell suspension was plated into 12 – well plates and cultured at 37 °C in a 5 % CO_2 incubator. For direct explantion of tissues, tissue pieces were placed into the center of 12 - well plate wells with cell culture medium. Due to considerably better isolation of cells from tissue explants, tissues from time points 3, 6 and 9 were subsequently used only as tissue explants and were cultured at 37 °C in a 5 % CO2 incubator. Cell culture medium was changed every 2–3 days. Explants were observed daily to monitor the appearance of live cells. Isolation of cells from tissue explants at time point 0 served as positive

control. All cell experiments were repeated 3 times - 3 different male mice for each time-point (3, 6 or 9 days after death) and storage conditions (4°C or room temperature).

RNA isolation

RNA isolation was performed from the cells isolated from muscle, hippocampus and subventricular zone tissues. All samples were stored at 4 °C for 3 days after death. After 80 - 90 % confluence was reached, cells were detached using cell scrapper. Cell suspension was removed from the wells and centrifuged at 240 rcf/min for 4 minutes. Pellet of cells was resuspended in DPBS and centrifuged again. Total RNA extraction was carried out using Trizol (Invitrogen, USA) according to manufacturer's protocol. The amount of extracted total RNA was measured by UV spectrophotometer (Thermo Scientific, USA) at 260/280 nm wave length.

Reverse transcription quantitative polymerase chain reaction

Following RNA isolation, reverse transcription quantitative polymerase chain reaction was performed. Reverse transcription was carried out on 2 samples from each tissue source (muscle, hippocampus and subventricular zone). In the first step, 66.5 ng and 100 ng of total RNA of brain and muscle tissue, respectively, was reverse transcribed into cDNA using High Capacity cDNA Reverse Transcription Kit with RNAse Inhibitor (ThermoFisher) according to the manufacturer's protocol. Negative reverse transcription controls were included. All reactions were conducted in a total volume of 20 µL. Conditions for reverse transcription were as suggested in the manufacturer's protocol: 25°C for 10 minutes, 37°C for 120 minutes, 85°C for 5 minutes. Due to very low amount of isolated RNA, 100 ng of total RNA of each muscle sample was amplified using RT² PreAMP cDNA Synthesis Kit (Qiagen, USA) prior to quantitative polymerase chain reaction. In the second step RT² Profiler™ PCR Array for mouse cell lineage identification (Qiagen, USA) was performed. All RT² Profiler™ PCR Array amplifications were conducted in a total volume of 25 µL. For brain tissue, 66,5 ng cDNA was used as a template. For muscle tissue, 100 ng cDNA amplified with RT² PreAMP cDNA Synthesis Kit (Qiagen) was used as a template. The amplification was carried out in 96 - well RT2 Profiler PCR array plates (Qiagen) with a Light Cycler 96 (Roche Life Science) using the following program: 50 °C for 2 minutes, 95 °C for 10 minutes, and 45 cycles at 95 °C for 15 seconds, 60 °C for 60 seconds. List of gene symbols and names according to Mouse Cell Lineage Identification RT2 Profiler PCR Array is presented in table 1.

Results

Cell isolation at time point 0

Dissected tissues (adipose, muscle and brain tissue from hippocampus and subventricular zone) at time point 0 after death were first used for determination of a better method for cell isolation. Considerably fewer cells were obtained from enzymatically-digested tissues that yielded viable cells only occasionally compared to the tissues that were used as explants. Isolation of cells from tissue explants at time point 0 therefore served as positive control. In all four positive control tissues (adipose, muscle and brain tissue from hippocampus and subventricular zone), viable cells were obtained.

Cell isolation at 3, 6 and 9 days after death

In all instances at all time points cells were isolated only when tissue pieces or cadavers were stored at 4 °C. No cells were obtained from cadavers or tissue pieces when stored at room temperature. Cells from 3, 6 and 9 days after death were first observed 5 to 15 days after tissue explants were placed in the tissue culture, depending on the time of storage. Earlier observation of cell isolation correlated with earlier time point of tissue explants being placed in the tissue culture. Three days after death, viable cells were obtained from muscle tissue (Figure 1), brain tissue - hippocampus (Figure 2) and subventricular zone (Figure 3), but not from the adipose tissue. Cells from all brain tissues and muscle tissue stored as whole cadavers were obtained from all samples whereas cells from muscle tissue stored as tissue pieces were obtained in 1 out of 3 samples. Six days after death, live cells were obtained only occasionally, when stored at 4 °C. Cells from muscle tissue were obtained in 2 out of 3 samples stored as

Table 1: Gene symbols and names according to Mouse Cell Lineage Identification RT2 Profiler PCR Array

Gene symbol	Gene name	Gene symbol	Gene name
Alb	Albumin	***Krt14***	Keratin 14
Apoh	Apolipoprotein H	***Krt19***	Keratin 19
Aqp1	Aquaporin 1	***Lefty1***	Left right determination factor 1
Bmp4	Bone morphogenetic protein 4	***Map3k12***	Mitogen-activated protein kinase kinase kinase 12
Ccr5	Chemokine (C-C motif) receptor 5	***Miox***	Myo-inositol oxygenase
Cd34	CD34 antigen	***Mixl1***	Mix1 homeobox-like 1 (Xenopus laevis)
Cd3e	CD3 antigen, epsilon polypeptide	***Msln***	Mesothelin
Cd79a	CD79A antigen (immunoglobulin-associated alpha)	***Myh1***	Myosin, heavy polypeptide 1, skeletal muscle, adult
Chat	Choline acetyltransferase	***Myh11***	Myosin, heavy polypeptide 11, smooth muscle
Col10a1	Collagen, type X, alpha 1	***Myh7***	Myosin, heavy polypeptide 7, cardiac muscle, beta
Comp	Cartilage oligomeric matrix protein	***Myl3***	Myosin, light polypeptide 3
Cpa1	Carboxypeptidase A1	***Nanog***	Nanog homeobox
Ctsk	Cathepsin K	***Neurod1***	Neurogenic differentiation 1
Dcn	Decorin	***Neurog2***	Neurogenin 2
Dcx	Doublecortin	***Nkx2-2***	NK2 transcription factor related, locus 2 (Drosophila)
Dnmt3b	DNA methyltransferase 3B	***Nppa***	Natriuretic peptide type A
Dpp4	Dipeptidylpeptidase 4	***Olig2***	Oligodendrocyte transcription factor 2
Eno1	Enolase 1, alpha non-neuron	***Otx2***	Orthodenticle homolog 2 (Drosophila)
Fabp7	Fatty acid binding protein 7, brain	***Pdgfra***	Platelet derived growth factor receptor, alpha polypeptide
Fgf5	Fibroblast growth factor 5	***Podxl***	Podocalyxin-like
Foxa1	Forkhead box A1	***Pou4f2***	POU domain, class 4, transcription factor 2
Foxd3	Forkhead box D3	***Pou5f1***	POU domain, class 5, transcription factor 1
Foxg1	Forkhead box G1	***Prom1***	Prominin 1
G6pc	Glucose-6-phosphatase, catalytic	***Ptcra***	Pre T-cell antigen receptor alpha
Gad1	Glutamic acid decarboxylase 1	***Rcvrn***	Recoverin
Gad2	Glutamic acid decarboxylase 2	***Runx1***	Runt related transcription factor 1
Galc	Galactosylceramidase	***Ryr2***	Ryanodine receptor 2, cardiac
Gata1	GATA binding protein 1	***Sftpb***	Surfactant associated protein B
Gata2	GATA binding protein 2	***Sftpd***	Surfactant associated protein D
Gata6	GATA binding protein 6	***Slc17a6***	Solute carrier family 17 (sodium-dependent inorganic phosphate cotransporter), member 6
Gbx2	Gastrulation brain homeobox 2	***Slc17a7***	Solute carrier family 17 (sodium-dependent inorganic phosphate cotransporter), member 7
Gdf3	Growth differentiation factor 3	***Slc2a2***	Solute carrier family 2 (facilitated glucose transporter), member 2
Gfap	Glial fibrillary acidic protein	***Slc32a1***	Solute carrier family 32 (GABA vesicular transporter), member 1
Hand1	Heart and neural crest derivatives expressed transcript 1	***Smtn***	Smoothelin
Hand2	Heart and neural crest derivatives expressed transcript 2	***Sox17***	SRY-box containing gene 17
Hes5	Hairy and enhancer of split 5 (Drosophila)	***Sox2***	SRY-box containing gene 2
Hnf4a	Hepatic nuclear factor 4, alpha	***Sox7***	SRY-box containing gene 7
Ibsp	Integrin binding sialoprotein	***T***	Brachyury
Igf2	Insulin-like growth factor 2	***Tat***	Tyrosine aminotransferase
Ins2	Insulin II	***Tyr***	Tyrosinase
Itgb4	Integrin beta 4	***Zfp42***	Zinc finger protein 42
Krt10	Keratin 10	***Zic1***	Zinc finger protein of the cerebellum 1

whole cadavers and in 1 out of 3 samples stored as tissue pieces. Cells from hippocampus tissue were obtained in 1 out of 3 samples stored as whole cadavers and in 1 out of 3 samples stored as tissue pieces. Cells from subventricular zone were obtained in 1 out of 3 samples stored as whole cadavers. Nine days after death live cells were obtained in one sample from hippocampus tissue of one mouse, stored as a cadaver at 4°C. No difference in cell isolation at any time point was observed in regard whether tissue was obtained from the cadavers, or was stored as tissue pieces in PBS. Results of successful harvesting of cells from tissue explants are presented in table 2.

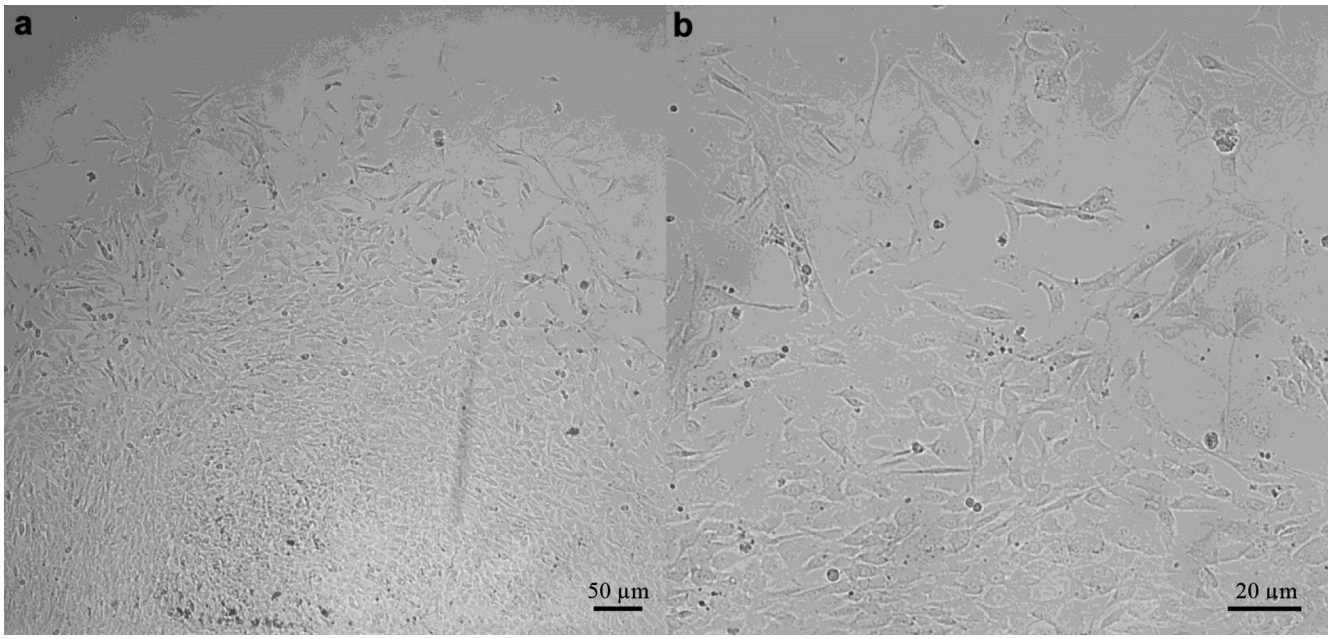

Figure 1: Cell isolation from muscle tissue stored at 4°C for 3 days, 17 days after seeding. A: cells coming out of muscle tissue explant. B: The same image at larger magnification

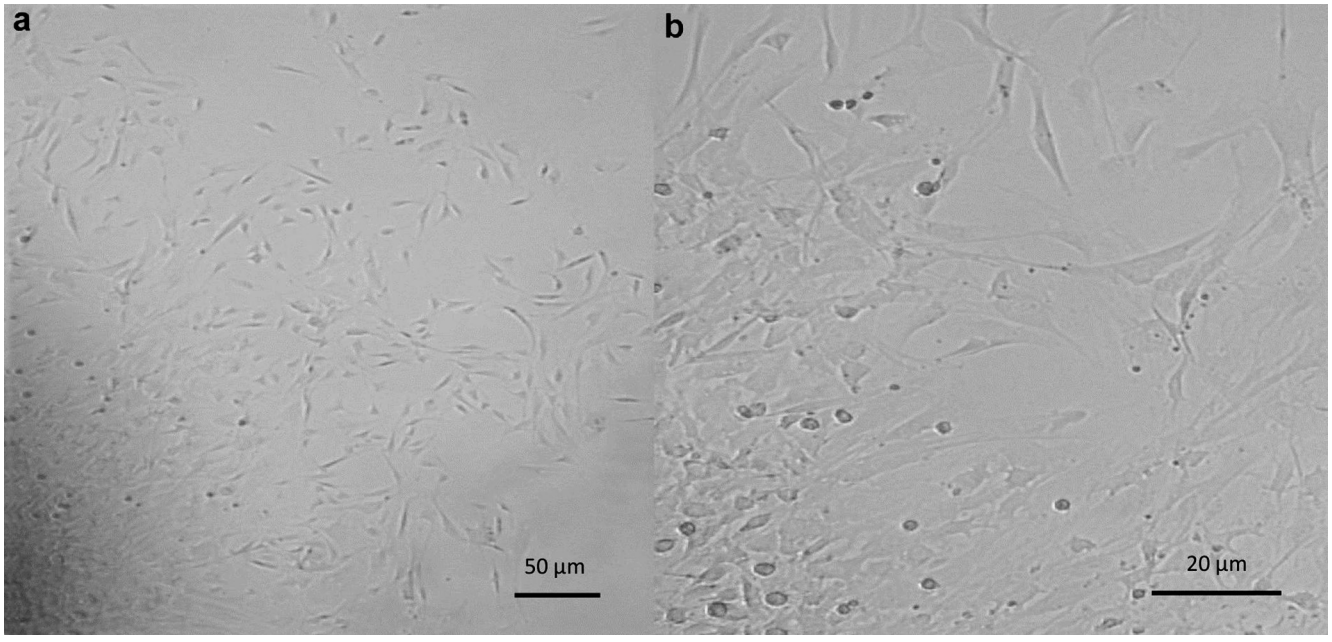

Figure 2: Cell isolation from brain tissue - hippocampus, stored at 4 °C for 3 days, 15 days after seeding. A: cells coming out of hippocampus tissue explant. B: The same image at larger magnification

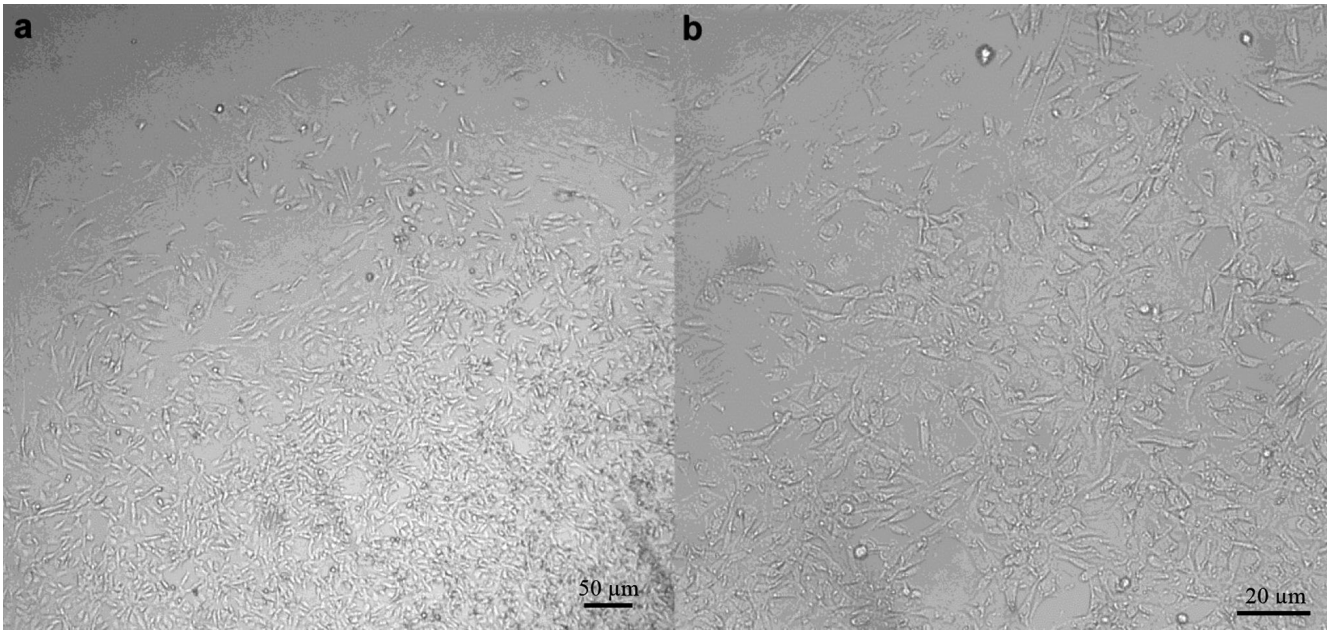

Figure 3: Cell isolation from brain tissue - subventricular zone, stored at 4 °C for 3 days, 15 days after seeding. A: cells coming out of brain tissue explant. B: The same image at larger magnification

Table 2: Number of samples from which cells were obtained regarding post mortem time points of tissue explantion, tissue type, storage temperature and form of tissue storage

		Days / Tissue	0	3	6	9
Tissue pieces stored in PBS	**4°C**	Muscle tissue	3/3	3/3	1/3	0/3
		Adipose tissue	3/3	0/3	0/3	0/3
		Subventricular zone	3/3	3/3	0/3	0/3
		Hippocampus	3/3	3/3	1/3	0/3
	Room temperature	Muscle tissue		0/3	0/3	0/3
		Adipose tissue		0/3	0/3	0/3
		Subventricular zone		0/3	0/3	0/3
		Hippocampus		0/3	0/3	0/3
Stored cadavers	**4°C**	Muscle tissue		1/3	2/3	0/3
		Adipose tissue		0/3	0/3	0/3
		Subventricular zone		3/3	1/3	0/3
		Hippocampus		3/3	1/3	1/3
	Room temperature	Muscle tissue		0/3	0/3	0/3
		Adipose tissue		0/3	0/3	0/3
		Subventricular zone		0/3	0/3	0/3
		Hippocampus		0/3	0/3	0/3

mRNA expression in isolated cells

Mouse Cell Lineage Identification RT2 Profiler PCR Array was used to profile the expression of 84 key genes for cellular differentiation with positive PCR controls included. Genes, for which Ct value was 35 or lower, were marked as genes expressed. In muscle tissue, mesoderm germ layer markers Dcn, Gata2, Pdgfra and Runx1 were expressed. Further, Cd79a, Ptcra and Cd34, mesoderm progenitor markers of early B and T cells and muscle stem cells were expressed, respectively. Of mesoderm terminal differentiation markers, genes encoding smooth muscle cells, osteoclasts and

Table 3: Genes expressed in cells isolated from muscle and brain tissue. Genes for which Ct value was 35 or lower, were marked as genes expressed. Genes expressed in cells isolated from muscle tissue are marked in purple. Genes expressed in cells isolated both from muscle and brain tissue are highlighted in blue

GENE ORIGIN	GENE SYMBOL
Pluripotency markers	
Pluripotency markers	Dnmt3b, Gdf3 (Vgr - 2), Lefty1, Nanog, Podxl, Pou5f1 (Oct4), Zfp42
Germ layers	
Ectoderm	Fgf5, Foxd3, Otx2, **Zic1**
Neuroectoderm	Gbx2, Neurog2
Mesoderm	Bmp4, Cd34, **Dcn, Gata2**, Hand1, Igf2, Mixl1, **Pdgfra, Runx1**, Brachyury
Endoderm	Foxa1, Gata1, **Gata6**, Hnf4a, Sox17, Sox7
Ectoderm progenitors	
Neuronal Progenitors	Fabp7, Hes5, Prom1, Sox2
Immature Neurons	Dcx
Immature GABA Neurons	**Gad2**, Slc32a1
Limbal Progenitors	**Eno1**, Msln
Motor Neuron Progenitors	Foxg1, Olig2
Oligodendrocyte Progenitors	Nkx2-2, Olig2
Mesoderm progenitors	
Early Cardiomyocytes	Hand2
Early B Cells	**Cd79a**
Early T Cells	Cd3e, **Ptcra**
Muscle Stem Cells	**Cd34**
Endoderm Progenitors	
Pancreatic Islet Cells	Krt19
Hepatic Stem Cells	**Apoh**, Dpp4, **Map3k12**
Ectoderm Terminal Differentiation Markers	
Keratinocytes	Krt10, Krt14
Melanocytes	Tyr
Mature Neurons	Neurod1
Cholinergic Neurons	Chat
GABA Neurons	Gad1
Glutamatergic Neurons	Slc17a6, Slc17a7
Astrocytes	**Galc**, Gfap
Ganglion Cells	Pou4f2
Photoreceptor Cells	**Rcvrn**
Mesoderm Terminal Differentiation Markers	
Skeletal Muscle Cells	Myh1
Smooth Muscle Cells	**Myh11, Smtn**
Cardiomyocytes	Myl3, Myh7, Nppa, Ryr2
Osteoblasts	Ibsp
Osteoclasts	**Ctsk**
Chondrocytes	Col10a1, **Comp**
Macrophages	Ccr5
Endoderm Terminal Differentiation Markers	
Hepatocytes	Alb, G6pc, **Tat**
Cholangiocytes	Itgb4
Beta Cells	Ins2, Slc2a2
Exocrine Cells	Cpa1
Lung Cells	Sftpb, Sftpd
Proximal Tubule Cells	Aqp1, Miox

chondrocytes were expressed. In addition to genes of mesodermal lineages, some genes of ectoderm and endoderm lineages were also expressed (Zic1, Gata6, Gad2, Eno1, Apoh, Map3k12, Galc, Rcvrn and Tat). In brain tissue, only expression of two genes was detected. In subventricular zone, gene Eno1, an ectoderm progenitor marker of limbal progenitors was expressed and in hippocampus, gene Rcvrn, an ectoderm terminal differentiation marker of photoreceptor cells was expressed. Results of gene expression from muscle and brain tissue derived cells are presented in table 3.

Discussion

In the present study, we examined the differences between time after death, storage temperature and form of tissue storage in obtaining live cells from mice post mortem. Results of our study suggest that cells from muscle and brain tissue can be isolated from murine cadavers or tissue pieces up to 3 days post mortem and with difficulty up to 6 days post mortem. Cells from brain tissue can possibly be isolated even up to 9 days post mortem. Several other studies have also shown that cells from brain and muscle tissue can be isolated from cadavers from different species after different post mortem periods. The longest post mortem time period that still allows for cell isolation from muscle tissue was reported by Latil et al. (12) who showed that viable and functional murine skeletal myogenic cells can be isolated up to 14 days post mortem. Interestingly, this is much longer time period in which cells were isolated post mortem compared to our study. But similarly as in our study, it was shown by Xu et al. (7) that neural stem cells of subventricular zone from deceased rats can also be isolated for up to 6 days post mortem, but not longer, in young rats. Time period in which cells were isolated was longer in young in comparison to old rats. In our study adult mice were used. It is possible that mice age in our study shortened the post mortem time periods in which cells were isolated as in most previous studies including study by Latil et al. (12) younger mice were used. Contrary to rodent neuronal stem cells, cells from human brain tissue are reported to be able to survive only up to 36 hours post mortem (15, 16), which suggests that post mortem time periods of neuronal stem cells from rodents might be longer than that of humans. This suggests that for some cell types post mortem time period of cell isolation might be species specific. Contrary, some studies indicate that post mortem time period might also be tissue specific. For example, it was shown by Latil et al. (12) that the longest post mortem time period of cell isolation from human muscle tissue was 17 days, which means it was not only similar to but it even exceeded the time period in which murine cells were isolated. Furthermore, it was shown by Erker et al. (5) that post mortem time periods of isolated hepatocytes do not differ between murine, rhesus macaque monkeys and humans. The lack of studies to compare post mortem isolation of cells from different species and tissues and different methods used in studies hinder speculation whether certain post mortem time period of cell isolation is species or tissue specific.

To our knowledge there are no studies in which comparison of different tissues regarding post mortem cell isolation from one species were studied. In our study, no significant difference was observed regarding post mortem time period for isolation of cells from brain and muscle tissue. In addition to brain, muscle and liver tissue, cells from other tissues have also been isolated post mortem, such as human retinal progenitor cells (immediately post mortem) (17), murine vestibular and cochlear stem cells (up to 10 days post mortem) (6), equine ligament stem cells (up to 72 hours post mortem) (11) and bovine skin fibroblast like cells (up to 49 days post mortem) (10).

Interestingly there are no reports of adipose tissue derived cells isolated post mortem, although adipose tissue is an excellent source of mesenchymal stem cells/multipotent mesenchymal stromal cells in different species. In our study adipose tissue yielded cells only immediately post mortem, but no cells were isolated at other time points after death, suggesting that cells in adipose tissue do not survive long after death. One possible reason for unsuccessful harvesting of adipose derived cells from mice post mortem in our study could be unsuitable anatomical site from which adipose tissue was obtained, since it was shown that there are intrinsic differences in adipocyte precursor cells from different white fat depots in mice (18) and that the concentrations of adipose derived stem cells from human cadavers differ between sites (19). Several studies have also shown that anatomical site of adipose tissue harvesting from live organisms is an important factor in terms of

differentiation potential, viability, yield and stem cell capacity (20–23), although there are no studies available comparing adipose tissue harvesting from different anatomical sites from BALB/C mice. Effect of different anatomical origins of adipose tissue on stem cell features could also reflect in the possibility of cells being harvested post mortem, although no studies are available on this topic. Another reason for unsuccessful obtaining of adipose derived cells could be in the adipose tissue differences between inbred mouse strains, as was shown in a study by Mo et al. (24), who compared the frequency of proliferative stromal cells in 129x1/svj and C57Bl/6J mice. But comparison of adipose derived cell characteristics between BALB/C and other mouse strains is yet to be studied.

In the present study, cells from muscle and brain tissues were isolated only when tissue pieces or cadavers were stored at 4°C. No cells were obtained from cadavers or tissue pieces when stored at room temperature, suggesting that low temperatures preserve the cells in cadavers or tissue pieces while higher (room) temperatures promote cell death. In most studies where post mortem cell isolation was examined, cells were harvested immediately after death for donor transplantation procedures (2–4, 25), or after longer periods of time after cadavers were stored at 4°C (5, 7). Interestingly, in some cases, where cells were successfully isolated from murine inner ear and human muscle tissue or arteries long after death, cadavers were kept at room temperature from 6 to 12 hours before they were stored at lower temperatures for later harvesting of cells (6, 12, 13), suggesting that shorter period at room temperature is compatible with obtaining viable cells while longer periods (as in our study) decrease the viability of cells in cadavers. Interestingly, in a recent study fibroblast - like cells were recovered up to 15- and 49-days postmortem from bovine skin stored at 25°C and 4°C, respectively (10). Although we were unable to obtain live cells when cadavers or tissue pieces were stored at room temperature, it seems that in some cases, stem cells can survive even after cadavers are stored for certain time periods at room temperature.

In most of the studies where cells were harvested at certain time points after death, animal or human subjects were stored in cadaveric form. In others, cadavers were dissected prior to experiment and tissue pieces were stored. There are, however, no studies in which affect of form of storage on cell isolation was investigated in the same study. In our study, no difference in cell isolation between two forms of storage was observed.

To find out which cells were isolated in our study, we used Mouse Cell Lineage Identification RT2 Profiler PCR Array that profiles the expression of 84 key genes for cellular differentiation. Array contains gene markers for specific cell types throughout cellular lineage progression, including pluripotent stem cells, progenitor cells from each of the three germ layers, and terminally differentiated cells. Results from qPCR suggests that from muscle and brain tissue, cells with characteristics of germ layer cells, progenitor cells and terminally differentiated cells were isolated. Cells obtained from brain tissue seem to be ectodermal progenitors and ectodermal terminally differentiated cells. In cells isolated from muscle tissue there was the strongest expression of markers for mesoderm germ layer, mesoderm progenitors and mesoderm terminally differentiated cells. However, cells isolated from muscle tissue also expressed some genes from ectodermal and endodermal lineages, possibly suggesting that heterogenous population of cells was obtained from muscle tissue. In general expression of all markers was low, possibly due to low amount of RNA obtained from the cells, and genes that were expressed in these cells were heterogenous. Therefore, it was not possible to exactly determine the lineage of cells obtained from dead mice, possibly suggesting that different types of cells were obtained, and further studies will be needed to more carefully examine the lineage and characteristic of cells obtained post mortem.

Despite the fact that heterogenic lineage population of cells from muscle tissue was isolated, it was concluded that, regardless of their origin, cells can be readily isolated from muscle and brain tissue 3 days post mortem. Although with difficulty, cells from muscle and brain tissue can also be isolated up to 6 days post mortem, and possibly even up to 9 days post mortem from brain tissue. Our results are consistent with results of other studies that showed that cells survive in the dead organisms for longer time after death than it was previously thought. In majority of the studies focusing on post mortem cell isolation, stem cells were obtained. It is presumed that, for example in satellite cells, the lack of oxygen, nutrients, or the

presence of extensive necrosis triggers a cellular response in stem cells resulting in their adopting a deeper state of quiescence or dormancy (12). Similarly, the possibility of post mortem neural stem cell isolation is ascribed to low metabolic level of neuronal stem cells and rich vascular bed in subventricular zone and surrounding tissues (7), which could act as a niche for neuronal stem cells (15). Hypoxia, which is prevalent in muscle stem cell niches (27) as well as in niches of other stem cells such as neuronal stem cells (28), is an important factor that contributes to cell viability and regeneration potential that could maintain stem cell viability for unusually long periods in spite of the necrotic microenvironment. Stem cells are thus assumed to be enriched in post mortem tissue due to cellular quiescence where cells adopt a reversible dormant state and thus possess a selective survival advantage compared with other cell types (12). Contrary to these studies we showed, based on gene expression results, that not only stem cells but also terminally differentiated cells survive in post mortem tissues for at least 3 days after death.

In conclusion, in this study we showed that (1) cells from murine animals can be isolated from muscle and brain tissue readily 3 days post mortem and with difficulty up to 6 days post mortem. Cells from brain tissue can possibly be isolated even up to 9 days post mortem (2). Compared to muscle and brain tissue no cells were isolated post mortem from adipose tissue except immediately after death (3). In all instances cells were isolated only when tissues were stored at 4 °C. 4) Form of tissue storage does not affect cell isolation (5). Not only stem cells but also terminally differentiated cells seem to survive in post mortem tissues for at least 3 days after death.

Acknowledgments

This study was supported by ARRS grant P4-0053 and Metka Voga is supported by ARRS Ph.D. fellowship. We are grateful to Nina Sterman for technical assistance.

The datasets supporting the results of this document are contained within the article. Any additional data may be requested to the corresponding author.

All animal experiments were approved by the Administration of the Republic of Slovenia for Food Safety, Veterinary Sector and Plant Protection of the Republic of Slovenia and were done according to ethical principles, EU directive (2010/63/EU), and NIH guidelines.

All authors declared that they have no competing interests.

MV and AP performed the experiments. GM planned the experiments and analyzed the data together with MV and AP. MV and GM drafted the manuscript, which was edited and approved by all authors.

References

1. Leming MR, Dickinson GE. Understanding dying, death, and bereavement. 4th. ed. Fort Warth : Harcourt Brace College Publishers, 1998: 518 str.

2. Blazar BR, Lasky LC, Perentesis JP, et al. Successful donor cell engraftment in a recipient of bone marrow from a cadaveric donor. Blood 1986; 67(6): 1655–60. doi: 10.1182/blood.V67.6.1655.1655

3. Ciancio G. Donor bone marrow infusion in cadaveric renal transplantation. Transplant Proc 2003; 35(2): 871–2. doi: 10.1016/s0041-1345(02)04034-4

4. Kapelushnik J, Aker M, Pugatsch T, Samuel S, Salvin S. Bone marrow transplantation from a cadaveric donor. Bone Marrow Transplant 1998; 21: 857–8. doi: 10.1038/sj.bmt.1701165

5. Erker L, Azuma H, Lee AY, et al. Therapeutic liver reconstitution with murine cells isolated long after death. Gastroenterology 2010; 139(3): 1019–29. doi: 10.1053/j.gastro.2010.05.082

6. Senn P, Oshima K, Teo D, Grimm C, Heller S. Robust postmortem survival of murine vestibular and cochlear stem cells. J Assoc Res Otolaryngol 2007; 8(2): 194–204. doi: 10.1007/s10162-007-0079-6

7. Xu Y, Kimura K, Matsumoto N, Ide C. Isolation of neural stem cells from the forebrain of deceased early postnatal and adult rats with protracted post-mortem intervals. J Neurosci Res 2003; 74: 533–40. doi: 10.1002/jnr.10769

8. Silvestre MA, Saeed AM, Cervera RP, Escribá MJ, García-Ximénez F. Rabbit and pig ear skin sample cryobanking: Effects of storage time and temperature of the whole ear extirpated immediately after death. Theriogenology 2003; 59(5/6): 1469–77. doi: 10.1016/s0093-691x(02)01185-8

9. Okonkwo C, Singh M. Recovery of fibroblast-like cells from refrigerated goat skin up to 41 d of animal death. In Vitro Cell Dev Biol Anim 2015; 51(5): 463–9. doi: 10.1007/s11626-014-9856-9

10. Walcott B, Singh M, Hatti Kaul R. Recovery of proliferative cells up to 15- and 49-day post-mortem from bovine skin stored at 25 °C and 4 °C, respectively. Cogent Biol 2017; 3(1): e1333760. doi: 10.1080/23312025.2017.1333760

11. Shikh Alsook MK, Gabriel A, Piret J, et al. Tissues from equine cadaver ligaments up to 72 hours of post-mortem: a promising reservoir of stem cells. Stem Cell Res Ther 2015; 6: e253. doi: 10.1186/s13287-015-0250-7

12. Latil M, Rocheteau P, Chatre L, et al. Skeletal muscle stem cells adopt a dormant cell state post mortem and retain regenerative capacity. Nat Commun 2012; 3: e903. doi: 10.1038/ncomms1890

13. Valente S, Alviano F, Caivarella C, et al. Human cadavermultipotent stromal/stem cells isolated from arteries stored in liquid nitrogen for 5 years. Stem Cell Res Ther 2014; 5(1): e8. doi: 10.1186/scrt397

14. Pozhitkov AE, Neme R, Domazet-Loso T, et al. Tracing the dynamics of gene transcripts after organismal death. Open Biol 2017; 7(1): e160267. doi: 10.1098/rsob.160267

15. Palmer TD, Schwartz PH, Taupin P, Kaspar B, Stein SA,Gage FH. Progenitor cells from human brain after death. Nature 2001; 411(6833): 42–3. doi: 10.1038/35075141

16. Schwartz PH, Bryant PJ, Fuja TJ, Su H, O'Dowd DK, Klassen H. Isolation and characterization of neural progenitor cells from post-mortem human cortex. J Neurosci Res 2003; 74(6): 838–51. doi: 10.1002/jnr.10854

17. Klassen H, Ziaeian B, Kirov, II, Young MJ, Schwartz PH. Isolation of retinal progenitor cells from post-mortem human tissue and comparison with autologous brain progenitors. J Neurosci Res 2004; 77(3): 334–43. doi: 10.1002/jnr.20183

18. Macotela Y, Emanuelli B, Mori MA, et al. Intrinsic differences in adipocyte precursor cells from different white fat depots. Diabetes 2012; 61: 1691–9. doi: 10.2337/db11-1753/-/DC1

19. Kishi K, Imanishi N, Ohara H, et al. Distribution of adipose-derived stem cells in adipose tissues from human cadavers. J Plast Reconstr Aesthet Surg 2010; 63(10): 1717–22. doi: 10.1016/j.bjps.2009.10.020

20. Prunet-Marcassus B, Cousin B, Caton D, Andre M, Penicaud L,Casteilla L. From heterogeneity to plasticity in adipose tissues: Site-specific differences. Exp Cell Res 2006; 312(6): 727–36. doi: 10.1016/j.yexcr.2005.11.021

21. Chen L, Peng EJ, Zeng XY, Zhuang QY,Ye ZQ. Comparison of the proliferation, viability, and differentiation capacity of adipose-derived stem cells from different anatomic sites in rabbits. Cells Tissues Organs 2012; 196(1): 13–22. doi: 10.1159/000330796

22. Tsekouras A, Mantas D, Tsilimigras DI, Moris D, Kontos M, Zografos GC. Comparison of the viability and yield of adipose-derived stem cells (ascs) from different donor areas. In Vivo 2017; 31(6): 1229–34. doi: 10.21873/invivo.11196

23. Reumann MK, Linnemann C, Aspera-Werz RH, et al. Donor site location is critical for proliferation, stem cell capacity, and osteogenic differentiation of adipose mesenchymal stem/stromal cells: Implications for bone tissue engineering. Int J Mol Sci 2018; 19(7): e1868. doi: 10.3390/ijms19071868

24. Mo J, Srour EF, Rosen ED. The frequency of proliferative stromal cells in adipose tissue varies between inbred mouse strains. J Stem Cells Regen Med 2009; 5(1): 23–9. doi: 10.46582/jsrm.0501005

25. Michalova J, Savvulidi F, Sefc L, Forgacova K, Necas E. Cadaveric bone marrow as potential source of hematopoietic stem cells for transplantation. Chimerism 2011; 2(3): 86–7. doi: 10.4161/chim.2.3.17917

26. Gustafsson MV, Zheng X, Pereira T, et al. Hypoxia requires notch signaling to maintain the undifferentiated cell state. Dev Cell 2005; 9(5): 617–28. doi: 10.1016/j.devcel.2005.09.010

27. Mohyeldin A, Garzon-Muvdi T,Quinones-Hinojosa A. Oxygen in stem cell biology: a critical component of the stem cell niche. Cell Stem Cell 2010; 7(2): 150–61. doi: 10.1016/j.stem.2010.07.007

IZOLACIJA ŽIVIH CELIC IZ RAZLIČNIH TKIV MIŠI DO DEVET DNI PO SMRTI

M. Voga, A. Pleterski, G. Majdič

Izvleček: Nekatere raziskave kažejo, da je preživetje celic v truplih precej daljše, kot je bilo znano do sedaj. V naši raziskavi smo proučevali, kako na uspešnost izolacije živih celic po smrti miši vplivajo različen čas izolacije po smrti, vrsta tkiva (mišično, možgansko in maščobno), temperatura shranjevanja trupel ter oblika shranjenega tkiva (kot koščki tkiv ali kot celi kadavri). Izolacija in gojenje celic iz tkiv mrtvih miši sta potekali pod standardnimi pogoji. Da bi ugotovili, katerim celičnim linijam pripadajo izolirane celice, je bil del celic uporabljen za izolacijo RNK in nadaljno uporabo v sistemu identifikacije izvornih celičnih linij z verižno reakcijo s polimerazo v realnem času. Rezultati naše raziskave so pokazali, da je žive celice mogoče izolirati iz mišičnega in možganskega tkiva 3 dni po smrti, pogojno tudi do 6 dni po smrti. Iz možganskega tkiva je bilo žive celice mogoče izolirati tudi do 9 dni po smrti. Iz maščobnega tkiva je bilo celice mogoče izolirati zgolj takoj po smrti, ne pa tudi v kasnejših časovnih intervalih. V vseh primerih so bile celice izolirane samo v primeru shranjevanja tkiv pri 4 °C. Oblika shranjenega tkiva na izolacijo celic ni vplivala. Izolirane celice so pripadale različnim zarodnim plastem. Rezultati raziskave so pokazali, da je žive celice iz mišjih trupel mogoče izolirati tudi več dni po smrti.

Ključne besede: miš; truplo; matične celice; možgansko tkivo; mišično tkivo; maščobno tkivo

Slov Vet Res 2021: 58 (4): 137 – 45
DOI 10.26873/SVR-1205-2021
UDC 639.21.09:578.27:616.831-002:616-036.2:597.556.331.1

Original Research Article

THE FIRST OUTBREAK OF VIRAL ENCEPHALOPATHY AND RETINOPATHY IN FARMED SEA BASS (*Dicentrarchus labrax)* IN SLOVENIA

Rosvita Sitar[1], Tanja Švara[2], Aleksandra Grilc Fajfar[3], Sabina Šturm[2], Marko Cvetko[2], Irena Fonda[4], Mitja Gombač[2]*

[1]National veterinary institute, Veterinary Faculty, University of Ljubljana, Unit Nova Gorica, Pri hrastu 18, 5000 Nova Gorica, [2]Institute of pathology, wild animals, fish and bees, [3]Institute of microbiology and parasitology, Veterinary Faculty, University of Ljubljana, Gerbičeva 60, 1000 Ljubljana, [4] Fonda.si d. o. o., Liminjanska cesta 117, 6320 Portorož, Slovenia

*Corresponding author, E-mail: mitja.gombac@vf.uni-lj.si

Abstract: Viral encephalopathy and retinopathy (VER) is considered a serious disease of several marine fish species, caused by RNA virus belonging to the family *Nodaviridae*, genus *Betanodavirus*. The disease is spread almost worldwide and causes significant losses among diseased fish. It is characterised by vacuolation of the central nervous system and the retina.
In July 2018, behavioural abnormalities i.e. altered swimming, swirling and vertical floating as well as lethargy and anorexia were observed in farmed sea bass (*Dicentrarchus labrax*) in the Gulf of Piran (Slovenia), associated with significant mortality. The disease initially occurred in juvenile sea bass, but later market-sized fish also became affected. Diseased fish displayed ocular opacity and multifocal skin ulceration on the head. Emaciation in some fish was also evident. Histopathology revealed characteristic vacuolation in the brain and retina. Performing a RT-PCR and RT-qPCR techniques, we have identified and confirmed the presence of betanodavirus nucleic acid in ocular and brain tissues. In addition, concentrations of the causative agent of VER in spleen and kidney did result in significantly higher viral yield than expected. Phylogenetic analysis showed that Slovenian isolate belongs to RGNNV species of betanodaviruses. Based on the clinical signs, gross and typical microscopic lesions and results of molecular analyses, we can conclude that farmed sea bass from the Gulf of Piran were affected with VER. To the best of our knowledge, this is the first report of VER in Slovenia.

Key words: viral encephalopathy and retinopathy; betanodavirus; sea bass; histopathology; RT-qPCR

Introduction

Viral encephalopathy and retinopathy (VER), also termed as viral nervous necrosis (VNN), is a serious neuropathological disease of more than 50 fish species almost worldwide (1). It occurs mostly in marine environment, but the outbreaks in freshwater fish have also been reported (2, 3, 4). In marine aquaculture, VER is considered one of the most devastating infectious diseases (5), and sea bass (*Dicentrarchus labrax*) seems to be one of the most commonly and severely affected species (6). The disease affects mostly the larval and juvenile stages (1, 7), however, in several fish species, such as sea bass (8, 9) and grouper (*Epinephelus septemfasciatus*) (10), mass moralities have been also reported in adult and market-sized fish (1). Additionally, clinical signs and mortalities associated with VER were reported in wild fish species (11).

The causative agent is small (approximately 25 nm in diameter) spherical non-enveloped RNA virus, belonging to the genus *Betanodavirus* within family *Nodaviridae* (1, 12).

Based on the phylogenetic analysis of the RNA sequence of the T4 variable region, betanodaviruses have been clustered into four

Received: 4 September 2020
Accepted for publication: 7 July 2021

species, named striped jack nervous necrosis virus (SJNNV), red-spotted grouper nervous necrosis virus (RGNNV), barfin flounder nervous necrosis virus (BFNNV) and tiger puffer nervous necrosis virus (TPNNV) (13). It is reported that RGNNV exhibits the widest host range of warm water species (14, 15), including sea bass. Furthermore, two reassortants RGNNV/SJNNV and SJNNV/RGNNV have been described and reported to infect different fish species in Mediterranean (5, 16, 17, 18). Betanodaviruses have been often detected in apparently healthy wild marine fish (19, 20, 21).

VER is characterized by typical changes in swimming pattern associated with affected nervous system (15), such as whirling, spiralling or looping, erratic swimming, lying down on the bottom, keeping vertical positions, lying on their sides or belly up and body curved (8, 9, 10, 22). In addition, lethargy, changes in skin pigmentation, skin erosion in the head region, ocular opacity and exophthalmia have been described (8, 11). Histopathological findings, most commonly characterized by vacuolation and necrosis of nerve cells of the brain, retina and spinal cord, are remarkably consistent among the various affected fish species (15, 23).

In this paper we describe the first occurrence of VER in Slovenia, including clinical signs, gross pathology, histopathological lesions and the results of molecular diagnostic procedures. Some epidemiological aspects are also discussed.

Case presentation

Case history and clinical signs

In July 2018, abnormal swimming behaviour associated with heavy mortalities occurred in sea bass reared in floating cages in the Gulf of Piran. Affected fish showed erratic swimming, impulsive movements, swirling, belly up or keeping vertical position with either head or caudal peduncle upside. Some were laying on their sides and body curved. Moreover, lethargy, anorexia, change in skin pigmentation, endo– or exophthalmia, ocular opacity and congestion of the head were observed. The disease initially occurred in older juveniles (125 g) and later market-sized fish became affected. There was no significant mortality observed in younger juveniles (50 g). Sea bream (*Sparus aurata*) also remained clinically unaffected (Table 1).

The marine fish farm concerned is the only one in Slovenia with the annual production of 100 tons and had no history of VER. No vaccination was carried out at that time; the juveniles introduced into the farm in 2017 had already been vaccinated against *Listonella anguillarum*, but not against other pathogens. In fact, the number of introduced juveniles was higher than in previous years, yet the density was only about 4.7 kg/m^3. Otherwise, husbandry practices and epizootiology in the area in the year of the outbreak generally did not differ from previous years.

In spring 2018, only sea bream juveniles were introduced into the farm, while the last introduction of sea bass juveniles took place in autumn 2017. At the time of the disease outbreak, the water temperature exceeded 26°C.

The outbreak characterized by high losses lasted until the beginning of October 2018. The mortality firstly decreased in the population of juvenile sea bass (125 g) in the middle of September at the water temperature range 23–25°C. About two weeks later at water temperature below 20°C, the disease mitigated in adult sea bass as well (Figure 1). Nevertheless, after the mortality rate in autumn had decreased, abnormal swimming behaviour was still present in some fish and was regularly observed for months.

Gross pathology

Samples of clinically affected sea bass were collected from various cages of older juveniles

Table 1: Cumulative mortality, from July 1st to December 31st, 2018, of different fish populations in the fish farm

Fish species and category	**Adult sea bass**	**Adult sea bass**	**Juvenile sea bass**	**Juvenile sea bass**	**Juvenile sea bream**	**Juvenile sea bream**
An average weight on July 1st, 2018 [g]	870	300	125	50	110	20
Cumulative mortality from July 1st to December 31st, 2018 [%]	51	48	45	8	2	4

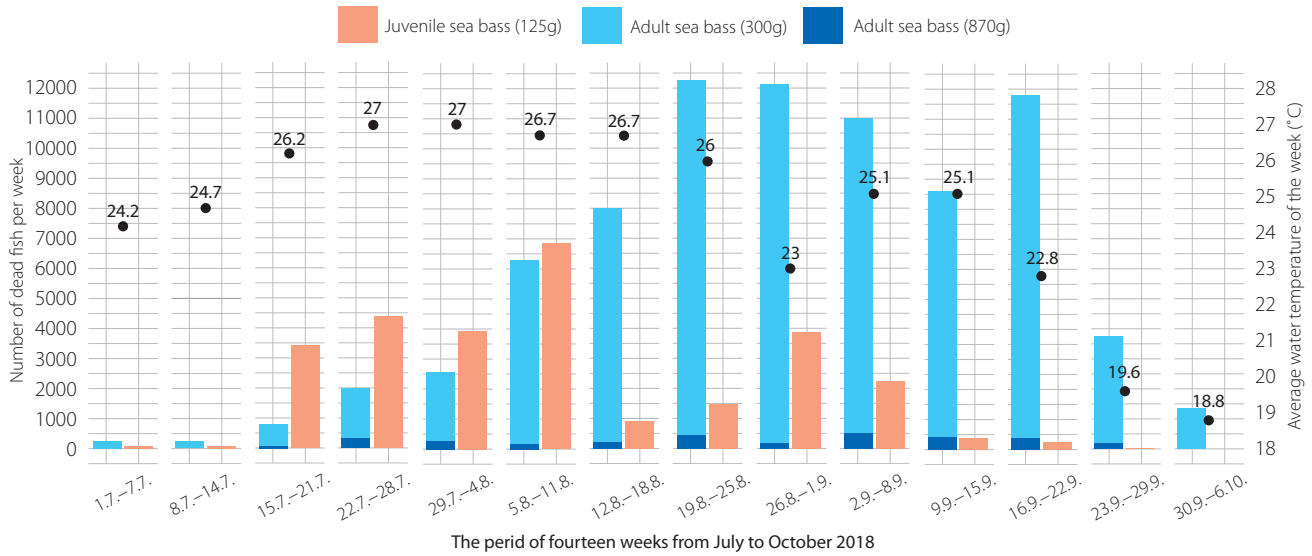

Figure 1: Disease pattern regarding the number of dead fish per week in most affected populations (juvenile sea bass (125 g) and adult sea bass (300 g and 870 g)) of sea bass at different sea temperature (an average weekly temperature)

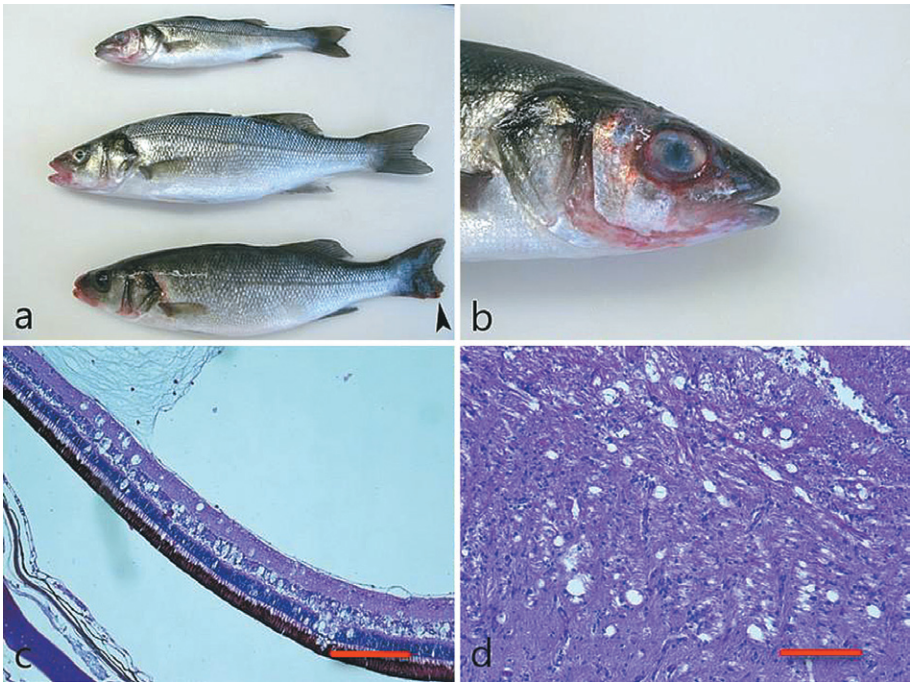

Figure 2: Viral encephalopathy and retinopathy. (a) Gross lesions included emaciation, ocular opacity and congestion of the head. In one fish, caudal fin erosion was noticed (arrowhead). (b) Close-up of the gross lesions showing ocular opacity and congestion on the head. (c) Characteristic vacuolation of the retina. HE. Scale bar: 100 µm; magnification: 100×. (d) Characteristic vacuolation in the neuropil of the brain. HE. Scale bar: 100 µm; magnification: 200×

(125 g) and adults (300 g). Seven fish (four older juveniles, three adults) were subjected for necropsy. External examination revealed lesions limited to the head, which consisted of multifocal skin ulceration and congestion, ocular opacity, exophthalmia or endophthalmia (Figures 2a, b). Additionally, one fish was emaciated, and caudal fin erosion was evident in another one (Figures 2a). No lesions were observed with examination of internal organs.

Histopathology

Eye and brain samples were fixed in 10% buffered formalin and routinely embedded in paraffin for histopathological examination. Four-µm thick tissue sections were first deparaffinised and then stained with haematoxylin and eosin (HE). Stained sections were examined with a light microscope. Microscopically, characteristic vacuolation in the retina and the brain was observed at different

degrees (Figures 2c, d). Brain vacuolation was mostly present in the neuropil and only single vacuoles were found in the neurons. Only in one fish, multifocal mild perivascular lymphocytic infiltrates and gliosis were found in the brain stem.

Virological analysis

The brain tissue and eyes as well as spleen and kidney were pooled separately and submitted for laboratory viral diagnostics. Fish organ homogenates were screened for betanodavirus by RT-PCR and RT-qPCR following the methods documented by Nishizawa et al. (24) and the World Organisation for Animal Health (OIE) in Manual of Diagnostic Tests for Aquatic Animals (2016) (1). All tissue samples were stored at –75°C for future analysis. Total RNA was extracted from supernatant of the organ homogenates (samples) using QIAamp Viral RNA (Qiagen, Germany). The extraction procedure was performed following the manufacturer's instructions. The RNA obtained was eluted in RNAse-free water. As a negative control, pool of negative fish tissue was processed alongside the virus isolate. Total RNA was added to a one-step RT-PCR for amplification of the certain genomic region within coat protein gene. A 427 nucleotide (nts) region targeting the T4 variable region of the RNA2 segment from diagnostic cases was amplified (Figure 3). RT-qPCR method was also introduced in the laboratory diagnostics of VER/VNN. A part of the RNA2 segment of viral genome was successfully detected using specific primers and MGB probe following OIE standard protocol (1).

Using molecular method RT-PCR we detected the presence of viral nucleic acid of betanodavirus successfully. With the RT-qPCR method, specific viral RNA in clinical samples can be detected quickly and specifically. Ct values obtained ranged from 15.88 (brain and bulbus) to 25.65 (spleen and kidney).

Confirmation of the positive results by both molecular methods, specific RT-PCR amplicon length for RNA2 genome region and the Ct values for RT-qPCR, corresponded 100%.

The RNA2 segment of Slovenian betanodavirus isolate was sequenced and compared with known isolates from betanodavirus coat protein sequences from different countries and hosts. A partial sequence of coat protein of 286 nts was aligned and used in phylogenetic analysis.

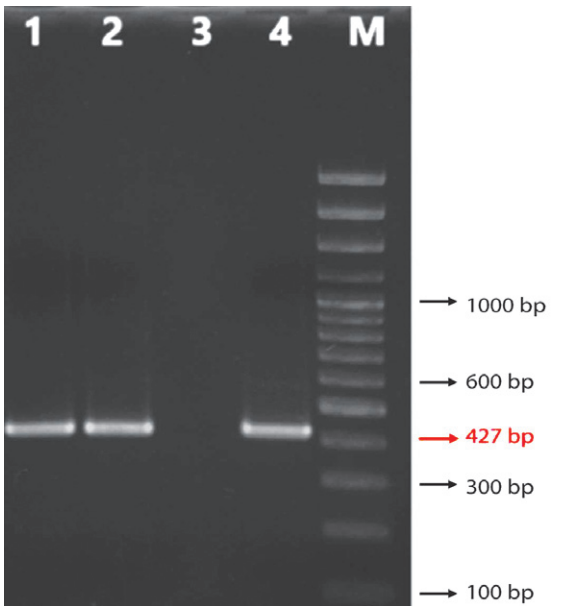

Figure 3: Agarose gel electrophoresis of RT-PCR positive samples of fish brain (1) and visceral organs (2) tested with F2/R3 primer pair. Reference negative (3) and positive (4) control. The red arrow indicates the expected size for the 427-bp amplicon. M = 100-bp size marker

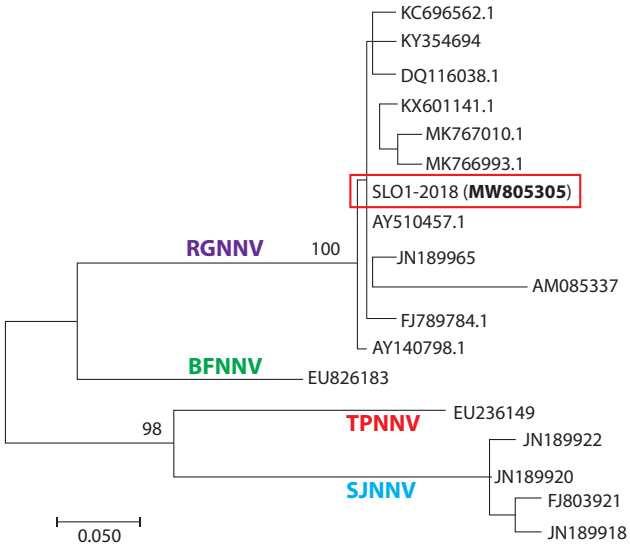

Figure 4: Maximum-likelihood (ML) phylogenetic tree based on partial RNA2 sequences depicting the phylogenetic relationships within genus *Betanodavirus*; subdivision of genus *Betanodavirus* is displayed by labeling the branches with different colors (violet: RGNNV; green: BFNNV; red: TPNNV; blue: SJNNV); ML bootstrap values >60% are reported next to the nodes; scale is shown at the left as substitutions per site.

Phylogenetic analysis was generated with the program MEGA version 7.0. and employed the Maximum-likelihood method using the Kimura two-parameter model (25) (Figure 4). The significance of the branching order was assessed

Table 2: Data related to the 18 betanodavirus isolates investigated in the phylogenetic analysis; abbreviations: unpubl., unpublished; n.d., data not available; t.s., this study

Isolate	Year of isolation	Country of outbreak	Reference	GenBank accession no.	Betanodavirus species
GMNNV-Korea	unknown	Korea	Cha et al., unpubl.(26)	DQ116038.1	RGNNV
9Gr.A.2012	2012	Greece	Bitchava et al., 2019(27)	MK767010.1	RGNNV
SpPm-IAusc1586.10	2010	Spain	Olveira et al., 2013(28)	KC696562.1	RGNNV
G9508KS	1995	Taiwan	Chi et al., 2003(29)	AY140798.1	RGNNV
28Gr.A.2013	2013	Greece	Bitchava et al., 2019(27)	MK766993.1	RGNNV
SFRG08/2013BSMu3	2013	Korea	Kim et al., unpubl.(30)	KX601141.1	RGNNV
570.16.2008c	2008	Italy	Panzarin et al., 2012(17)	JN189965	RGNNV
"1"	2009	Tunisia	Chérif et al., 2010(31)	FJ789784.1	RGNNV
"Redspotted grouper nervous necrosis virus"	unknown	China	Lin et al., unpubl.(32)	AY510457.1	RGNNV
Sa-I-97c	1997	Italy	Toffolo et al., 2007(33)	AM085337	RGNNV
VNNV/S. aurata/I/425-10/Sep2008	2008	Italy	Toffan et al., 2017(5)	KY354694	RGNNV
SpSa-IAusc156.03c 2003 Larvae	2003	Spain	Olveira et al., 2009(16)	FJ803921	SJNNV
37.2.2005c	2005	Portugal	Panzarin et al., 2012(17)	JN189918	SJNNV
250.1.2009c	2009	Cyprus	Panzarin et al., 2012(17)	JN189920	SJNNV
292.1.2.2009c	2009	Greece	Panzarin et al., 2012(17)	JN189922	SJNNV
BF93Hok	unknown	Japan	Nerland et al., unpubl.(34)	EU826138	BFNNV
TPKag93	unknown	Japan	Okinaka, unpubl.(35)	EU236149	TPNNV
SLO1-2018	2018	Slovenia	t.s.	MW805305	RGNNV

by bootstrap resampling of 1000 replicates. Accession numbers of nucleotide sequences for VER/VNN worldwide isolates available at GenBank were cited and listed in Table 2.

Based on clinical signs, typical histopathological lesions followed by identification of the causative agent by molecular analysis, VER was diagnosed.

Discussion

Since late 80', mass mortalities in farmed sea bass showing abnormal swimming behaviour have been reported from Mediterranean region by several authors (8, 9, 36). In summer 1995, heavy losses associated with nodavirus infection occurred in juvenile and adult sea bass in several marine fish farms in Italy (9) and VER is currently considered to be endemic in Mediterranean basin (5). However, in Slovenia altered swimming behaviour associated with mass mortalities in marine aquaculture fish species had not been observed until recently. Clinical signs as well as gross and histopathological findings in our case were similar to those described by other authors (8, 9, 22, 37, 38).

The temperature range at the time of the outbreak in July 2018 was in accordance with an optimal *in-vitro* growth temperature for betanodavirus species RGNNV at 25–30°C (39), and mortality significantly decreased at water temperature below 20°C.

The source of infection in our case is difficult to define, considering that only sea bream was introduced into the farm in 2018. Transmission of the disease occurs mainly horizontally through contaminated water (1), but vertical transmission has also been demonstrated in several fish species (7).

An additional possibility of transmission of the betanodavirus is represented from infected, asymptomatic specimens (21, 40). Results of infection trials reported by Castric et al. (41) showed that experimentally infected sea bream with no clinical signs of the disease was able to infect the juvenile sea bass by cohabitation. Furthermore, betanodavirus was detected in several marine invertebrate species, including Mediterranean mussel (*Mytilus galloprovincialis*) (42), which is the main cultured mollusc species in Slovenia. Moreover, the mollusc farming area Seča is in the immediate vicinity to the relevant fish farm. Kim et al. (43) confirmed infectivity of either BFNNVs or RGNNVs from shellfish, which may represent a potential risk for transmission of nodaviruses to cultured and wild host species. The ability of the sea bass nodavirus to survive at least one month at 25°C and at least one year at 15°C indicates that once released into the marine environment, it could remain widely spread during either cold or warm seasons (44). Thus, control measures possibly effective in hatcheries by implementation of proper disinfection procedures followed by introducing of betanodavirus-free broodstock, have limited results in preventing betanodavirus infections of farmed fish exposed to the marine environment in on-growing sites (15).

The nucleotide diversity of RGNNV isolates worldwide has been shown to vary depending on host species and environmental conditions (18, 45). Isolates from Italy, Spain, Portugal, Cyprus, Greece and Tunisia represent Mediterranean Basin.

Viral isolates collected from certain geographic area are generally similar to each other. In the present study, the most revealing spatial trend was the clear separation of isolates from the same geographical location. According to the genotype and geographical origin, SJNNV isolates within Mediterranean region and Japanese isolate from TPNNV species form two independent clusters.

Maximum-likelihood phylogenetic tree based on partial RNA2 sequences determined that the selected isolates within RGNNV species showed spatial correlation. In this study, geographic clustering of the virus isolates from Greece and Italy was observed. It is also important to note that within betanodavirus species RGNNV, closer phylogenetic relatedness of Korean RGNNV isolates with those from Greece and Italy was detected.

The determined partial T4 nucleotide sequence of Slovenian isolate showed 88.93 to 100% identity at the nucleotide level to the sequences among selected betanodavirus isolates analysed, highly related to strain RGNNV. The evolutionary analysis showed the phylogenetic relationships of newly characterized Slovenian isolate with the RGNNV species. Interestingly, it also exhibited 100% identity to the virus isolate from China.

In this study, the determined partial RNA2 segment sequences representing four major betanodavirus species showed 65.04 to 100% identity at the nucleotide level to the selected sequences of 18 worldwide betanodavirus isolates.

In our case high viral load was detected also in spleen and kidney. Retina and central nervous system including the brain and spinal cord are key organs of the infection in which the virus actively replicates. Kidney and spleen are not considered the target organs and therefore not suitable for VER diagnosis, but nevertheless causative agent of the disease can be detected in many organs according to published data (1). Our results revealed that besides bulbus and brain tissue kidney and spleen could also be suitable tissues for analysis.

Considering the severity of the disease and based on available data suggesting the immunogenic characteristics of the NNV in sea bass, great effort has been made in vaccine development (46), including attenuated, inactivated, recombinant and DNA vaccines with promising results (47).

Recently, an inactivated injectable vaccine against VER caused by RGNNV species for sea bass has been authorised for use in the appointed Mediterranean countries: Spain, Italy, Croatia and Greece (Pharmaq) (48). It is to be administered to fish of a minimum weight of 12 g, and the expected reduce of mortality caused by nodavirus (RGNNV species) in sea bass is up to 12 months post vaccination.

In these aspects, we believe that introduction of already vaccinated juveniles into Slovenian marine aquaculture facilities would be strongly recommended.

Conclusion

VER is one of the most devastating diseases of marine fish species with great impact on marine aquaculture. It is endemic in Mediterranean Basin, but the first outbreak in Slovenia occurred only in 2018. The disease caused increased mortality in juvenile and adult sea bass, which led to final loss of about 50% of affected populations. Phylogenetic analysis of Slovenian RGNNV isolate indicates its

close relation to other isolates from Mediterranean Basin. Subsequently, an authorised vaccine for selected Mediterranean countries could reduce the mortality rate and economic losses caused by VER also in sea bass in Slovenia.

References

1. Viral encephalopathy and retinopathy. In: OIE manual of diagnostic tests for aquatic animals. 7th ed. Paris : Office International des Epizooties, 2016: Chapter 2.3.12 https://www.oie.int/fileadmin/Home/eng/Health_standards/aahm/current/chapitre_viral_encephalopathy_retinopathy.pdf (June 2020)

2. Bigarré L, Cabon J, Baud M, et al. Outbreak of betanodavirus infection in tilapia, *Oreochromis niloticus* (L.), in fresh water. J Fish Dis 2009; 32: 667–73.

3. Bovo G, Gustinelli A, Quaglio F, et al. Viral encephalopathy and retinopathy outbreak in freshwater fish farmed in Italy. Dis Aquat Org 2011; 96: 45–54.

4. Binesh CP. Mortality due to viral nervous necrosis in zebrafish *Danio rerio* and goldfish *Carassius auratus*. Dis Aquat Org 2013; 104: 257–60.

5. Toffan A, Pascoli F, Pretto T, et al. Viral nervous necrosis in gilthead sea bream (*Sparus aurata*) caused by reassortant betanodavirus RGNNV/SJNNV: an emerging threat for Mediterranean aquaculture. Sci Rep 2017; 7: e46755. doi: 10.1038/srep46755

6. Toffan A. Viral encephalopathy and retinopathy. In: MedAID H2020 project blog. Mediterranean Aquaculture Integrated Development, 2018. http://www.medaid-h 2020.eu/index.php/2018/09/06/viral-encephalopathy-and-retinopathy/ (June 2020)

7. Munday BL, Kwang J, Moody N. Betanodavirus infections of teleost fish: a review. J Fish Dis 2002; 25: 127–42

8. Le Breton A, Grisez L, Sweetman J, Ollevier F. Viral nervous necrosis (VNN) associated with mass mortalities in cage-reared sea bass, *Dicentrarchus labrax* (L.). J Fish Dis 1997; 20: 145–51.

9. Bovo G, Nishizawa T, Maltese C, et al. Viral encephalopathy and retinopathy of farmed marine fish species in Italy. Virus Res 1999; 63: 143–6.

10. Fukuda Y, Nguyen HD, Furuhashi M, Nakai T. Mass mortality of cultured sevenband grouper, *Epinephelus septemfasciatus*, associated with viral nervous necrosis. Fish Pathol 1996; 31: 165–70.

11. Vendramin N, Patarnello P, Toffan, et al. Viral encephalopathy and retinopathy in groupers (*Epinephelus* spp.) in southern Italy: a threat for wild endangered species? BMC Vet Res 2013; 9: e20. doi: 10.1186/1746-6148-9-20

12. Mori KI, Nakai T, Muroga K, Arimoto M, Mushiake K, Furusawa I. Properties of a new virus belonging to nodaviridae found in larval striped jack (*Pseudocaranx dentex*) with nervous necrosis. Virology 1992; 187: 368–71.

13. Nishizawa T, Furuhashi M, Nagai T, Nakai T, Muroga K. Genomic classification of fish nodaviruses by molecular phylogenetic analysis of the coat protein gene. Appl Environ Microbiol 1997; 63: 1633–6.

14. Low CF, Syarul Nataqain B, Chee HY, Rozaini MZH, Najiah M. Betanodavirus: dissection of the viral cycle. J Fish Dis 2017; 40: 1489–96.

15. Doan QK, Vandeputte M, Chatain B, Morin T, Allal F. Viral encephalopathy and retinopathy in aquaculture: a review. J Fish Dis 2017; 40: 717–42.

16. Olveira JG, Souto S, Dopazo CP, Thiéry R, Barja JL, Bandín I. Comparative analysis of both genomic segments of betanodaviruses isolated from epizootic outbreaks in farmed fish species provides evidence for genetic reassortment. J Gen Virol 2009; 90: 2940–51.

17. Panzarin V, Fusaro A, Monne I, et al. Molecular epidemiology and evolutionary dynamics of betanodavirus in southern Europe. Infect Genet Evol 2012; 12: 63–70.

18. Toffan A, Panzarin V, Toson M, Cecchettin K, Pascoli F. Water temperature affects pathogenicity of different betanodavirus genotypes in experimentally challenged *Dicentrarchus labrax*. Dis Aquat Org 2016; 119: 231–8.

19. Barker DE, MacKinnon AM, Boston L, et al. First report of piscine nodavirus infecting wild winter flounder *Pleuronectes americanus* in Passamaquoddy Bay, New Brunswick, Canada. Dis Aquat Org 2002; 49: 99–105.

20. Gomez DK, Sato J, Mushiake K, Isshiki T, Okinaka Y, Nakai T. PCR-based detection of betanodaviruses from cultured and wild marine fish with no clinical signs. J Fish Dis 2004; 27: 603–8.

21. Giacopello C, Foti M, Bottari T, Fisichella V, Barbera G. Detection of viral encephalopathy and retinopathy virus (VERV) in wild marine fish species of the South Tyrrhenian Sea (Central Mediterranean). J Fish Dis 2013; 36: 819–21.

22. Grotmol S, Totland GK, Thorud K, Hjeltnes BK. Vacuolating encephalopathy and retinopathy

associated with a nodavirus-like agent: a probable cause of mass moirtality of cultured larval and juvenile Atlantic halibut *Hippoglossus hippoglossus*. Dis Aquat Org 1997; 29: 85–97.

23. Munday BL, Nakai T. Special topic review: nodaviruses as pathogens in larval and juvenile marine finfish. World J Microbiol Biotechnol 1997; 13: 375–81.

24. Nishizawa T, Mori KI, Nakai T, Furusawa I, Muroga K. Polymerase chain reaction (PCR) amplification of RNA of striped jack nervous necrosis virus (SJNNV). Dis Aquat Org 1994; 18: 103–7.

25. Kimura M. A simple method for estimating evolutionary rate of base substitutions through comparative studies of nucleotide sequences. J Mol Evol 1980; 16: 111–20.

26. Cha SJ, Do JW, Park JW. Coat protein of a Korean isolate of fish nodavirus from grey mullet (*Mugil cephalus*). GenBank: DQ116038.1. Bethesda : National Center for Biotechnology Information, U.S. National Library of Medicine, 30. Jul. 2005. https://www.ncbi.nlm.nih.gov/nuccore/DQ116038.1 (Feb. 2019)

27. Bitchava K, Chassalevris T, Lampou E, Athanassopoulou F, Economou V, Dovas CI. Occurrence and molecular characterization of betanodaviruses in fish and invertebrates of the Greek territorial waters. J Fish Dis 2019; 42: 1773–83.

28. Olveira JG, Souto S, Dopazo CP, Bandin I. Isolation of betanodavirus from farmed turbot Psetta maxima showing no signs of viral encephalopathy and retinopathy. Aquaculture 2013; 406/407: 125–30.

29. Chi SC, Shieh JR, Lin SJ. Genetic and antigenic analysis of betanodaviruses isolated from aquatic organisms in Taiwan. Dis Aquat Org 2003; 55: 221–8.

30. Kim YC, Jeong HD. Highly frequent identification of betanodavirus BFNNV as well as RGNNV genotype in shellfish. GenBank: KX575831.1. Bethesda : National Center for Biotechnology Information, U.S. National Library of Medicine, 29. Oct. 2016. https://www.ncbi.nlm.nih.gov/nuccore/KX575831.1 (Feb. 2019)

31. Cherif N, Gagne N, Groman D, Kibenge F, Iwamoto T, Yason C, Hammami S. Complete sequencing of Tunisian redspotted grouper nervous necrosis virus betanodavirus capsid gene and RNA-dependent RNA polymerase gene. J Fish Dis 2010; 33: 231–40.

32. Lin L, Huang J, Weng S, He J. Partial capsid protein gene of red-spotted grouper nervous necrosis virus in Guangdong province, P. R. China. GenBank AY510457.1. Bethesda : National Center for Biotechnology Information, U.S. National Library of Medicine, 26. Jul. 2016. https://www.ncbi.nlm.nih.gov/nuccore/AY510457.1 (Feb. 2019)

33. Toffolo V, Negrisolo E, Maltese C, et al. Phylogeny of betanodaviruses and molecular evolution of their RNA polymerase and coat proteins. Mol Phylogenet Evol 2007; 43: 298–308.

34. Nerland AH, Oevergaard A-C, Patel S, Nishizawa T. Complete sequence of RNA1 and RNA2 from the nodavirus strain BF93Hok isolated from barfin flounder, *Verasper moseri* at Hokkiado, Japan. GenBank: EU826138. Bethesda : National Center for Biotechnology Information, U.S. National Library of Medicine, 20. Jul. 2008. https://www.ncbi.nlm.nih.gov/nuccore/EU826138 (Feb. 2019)

35. Okinaka Y. Comparison among the complete genomes of the four types of Betanodaviruses. GenBank: EU236149. Bethesda : National Center for Biotechnology Information, U.S. National Library of Medicine, 1. Nov. 2009. https://www.ncbi.nlm.nih.gov/nuccore/EU236149 (Feb. 2019)

36. Breul G, Bonami JR, Pepin JF, Pichot. Viral infection (picorna-like virus) associated with mass mortalities in hatchery-reared sea-bass (*Dicentrarchus labrax*) larvae and juveniles. Aquaculture 1991; 97: 109–16.

37. Lopez-Jimena B, Garcia-Rosado E, Thompson KD, et al. Distribution of red-spotted grouper nervous necrosis virus (RGNNV) antigens in nervous and non-nervous organs of European seabass (*Dicentrarchus labrax*) during the course of an experimental challenge. J Vet Sci 2012; 13: 355–62.

38. Pascoli F, Serra M, Toson M, Pretto T, Toffan A. Betanodavirus ability to infect juvenile European sea bass, Dicentrarchus labrax, at different water salinity. J Fish Dis 2016; 39: 1061–8.

39. Iwamoto T, Nakai T, Mori K, Arimoto M, Furusava I. Cloning of the fish cell line SSN-1 for piscine nodaviruses. Dis Aquat Org 2000; 43: 81–9.

40. Terlizzi A, Tedesco P, Patarnello P. Spread of pathogens from marine cage aquaculture: a potential threat for wild fish assemblages under protection regimes? In: Carvalho ED, David GS, Silva RJ, eds. Health and environment in aquaculture. Rijeka : IntechOpen, 2012: 403–14. https://www.intechopen.com/books/health-and-environment-in-aquaculture (Feb. 2019)

41. Castric J, Thiéry R, Jeffroy J, de Kinkelin P, Raymond JC. Sea bream *Sparus aurata*, an

asymptomatic contagious fish host for nodavirus. Dis Aquat Org 2001; 47: 33–8.

42. Gomez DK, Baeck GW, Kim JH, Choresca Jr CH, Park SC. Molecular detection of betanodaviruses from apparently healthy wild marine invertebrates. J Invertebr Pathol 2008; 97: 197–202.

43. Kim YC, Kwon WJ, Kim MS, Kim KI, Min JG, Jeong HD. High prevalence of betanodavirus barfin flounder nervous necrosis virus as well as red-spotted grouper nervous necrosis virus genotype in shellfish. J Fish Dis 2018; 41: 233–46.

44. Frerichs GN, Tweedie A, Starkey WG, Richards RH. Temperature, pH and electrolyte sensitivity, and heat, UV and disinfectant inactivation of sea bass (*Dicentrarchus labrax*) neuropathy nodavirus. Aquaculture 2000; 185: 13–24.

45. Vendramin N, Toffan A, Mancin M, et al. Comparative pathogenicity study of ten different betanodavirus strains in experimentally infected European sea bass, *Dicentrarchus labrax* (L.). J Fish Dis 2014; 37: 371–83.

46. Miccoli A, Saraceni PR, Scapigliati G. Vaccines and immune protection of principal Mediterranean marine fish species. Fish Shellfish Immunol 2019; 94: 800–9.

47. Gonzales-Silvera D, Guardiola FA, Espinosa C, Chavez-Pozo E, Esteban MÁ, Cuesta A. Recombinant nodavirus vaccine produced in bacteria and administrated without purification elicits humoral immunity and protects European sea bass against infection. Fish Shellfish Immunol 2019; 88: 458–63.

48. Pharmaq. Pharmaq has received marketing authorizations (MA) for Nodavirus vaccine for European sea bass in Spain, Italy, Croatia and Greece. Oslo : Pharmaq, 2016. https://www.pharmaq.no/updates/pharmaq-has-rec/ (June, 2020)

PRVI IZBRUH VIRUSNE ENCEFALOPATIJE IN RETINOPATIJE PRI GOJENIH BRANCINIH (*Dicentrarchus labrax)* V SLOVENIJI

R. Sitar, T. Švara, A. Grilc Fajfar, S. Šturm, M. Cvetko, I. Fonda, M. Gombač

Izvleček: Virusna encefalopatija in retinopatija (VER) je nevarna bolezen številnih vrst morskih rib, ki jo povzroča nevrotropni RNA virus iz družine *Nodaviridae*, rod *Betanodavirus*. Bolezen je razširjena skoraj po vsem svetu in povzroča visok pogin okuženih rib. Zanjo so značilne vakuole v centralnem živčnem sistemu in retini. Konec julija 2018 so v ribogojnici v Piranskem zalivu pri brancinih opazili nepravilno plavanje, vrtenje in postavljanje v vertikalno smer ter letargijo in neješčnost, brancini so množično poginjali. Bolezen se je najprej pojavila pri mladicah, nato tudi pri konzumnih kategorijah brancinov. Obolele ribe so imele sivomotna očesna zrkla ter multifokalne kožne razjede na glavi, posamezne so bile shujšane. S histopatološko preiskavo smo ugotovili značilne vakuole v možganih in retini. Z molekularnima metodama RT-PCR in RT-qPCR smo potrdili prisotnost nukleinske kisline betanodavirusa v očesnem zrklu in možganih. Koncentracije virusa, ki so bile signifikantno višje od pričakovanih, smo ugotovili tudi v vranici in ledvicah. Na podlagi kliničnih znakov, makroskopskih in tipičnih histopatoloških sprememb ter rezultatov molekularnih preiskav lahko zaključimo, da so gojeni brancini v ribogojnici v Piranskem zalivu zboleli za VER. Opisani izbruh je prvi potrjeni primer te bolezni v Sloveniji.

Ključne besede: virusna encefalopatija in retinopatija; betanodavirus; brancin; histopatologija; RT-qPCR

Slov Vet Res 2021: 58 (4): 147 – 53
DOI 10.26873/SVR-1356-2021
UDC 599.742.734:591.421:572.7:591.8

Original Research Article

MORPHOLOGY AND HISTOLOGY OF THE EURASIAN LYNX (*Lynx lynx*) PLANUM NASALE

Hasan Hüseyin Ari[1,3], Sema Uslu[2]*

[1]Departments of Anatomy, [2]Departments of Histology and Embryology, Faculty of Veterinary Medicine, Sivas Cumhuriyet University, Sivas, Turkey, [3]Departments of Anatomy, Faculty of Veterinary Medicine, Kyrgyz-Turkish Manas University, Bishkek, Kyrgyzstan Republic

*Corresponding author, E-mail: semauslu43@hotmail.com

Abstract: This study reveals the macroscopic and microscopic structures of the Eurasian lynx planum nasale using materials from three dead females obtained from the Sivas Forestry Branch of Agriculture and Forestry Ministry of the Republic of Turkey. To accomplish the purpose, planum nasale was investigated using macroscopic, histological, and scanning electron microscopy (SEM) techniques. The microscopic examination showed that the planum nasale consists of hairless, moist, glabrous skin and resembles a ship anchor with arm, palm, stock, and sickle parts. The planum nasale's surface is formed by epidermal plates or epidermal ridges, which were separated from each other by primary and secondary fissures showed in SEM and macroscopic figures. Based on the microscopic examination, the Mercel's cells and nerve ends are located in the basal sheet of the planum nasale's epidermal layers. In addition, the pores situated on the surface of the epidermal ridges and the dense connective bundles were settled in the dermal layers, based on the SEM examination.

Key words: Eurasian lynx (*Lynx rufus*); morphology; nasal plane; planum nasale

Introduction

The Euroasian lynx (*Lynx lynx)* is an endangered species of wild animal (1). The species features of the lynx are medium size, a small head, a prominent ruff of fur, ears tipped with tufts of black hair, and long legs relative to its body length. The literature reports that the most distinguishing anatomical characteristic of these wild animals is the absence of a set upper premolar (2).

The planum nasale, which comes from a Latin word meaning the tip of the nose, is a well-studied anatomical and histological structure in various species (3, 4, 5, 6, 7). This anatomical structure is called the nasal plane (*planum nasale*) in carnivores and small ruminants but the nasolabial plane (*planum nasolabiale*) in large ruminants and the rostral plane (*planum rostrale*) in swine. The nasal plane is macroanatomically formed by glabrous skin and philtrum, different from other regions of the head (8, 9, 10, 11). The skin of the nasal plane includes medial nasal wings, which are differentiated for adaptation to different environments. The surface of the nasal plane skin exhibits a unique morphology that includes papillae or epidermal ridges (4, 5). The anatomical structure consists of the epidermal ridges, which are used as a nasal print (5, 12) because of the individual animal's characteristics throughout

Received: 5 July 2020
Accepted for publication: 12 November 2021

life (13, 14). Histologically, the planum nasale's skin consists of an epidermis and a dermis. In addition, Esrah (5) reported that skeleton muscle exists just below the dermis.

The morphology of the planum nasale has been compared between various species for many years. Despite several current studies on the anatomical structures of the Eurasian lynx (1, 15), to our knowledge, no anatomical descriptions of the nasal plane in the Eurasian lynx are available, so this study could present the first anatomical findings on the planum nasale obtained using light and scanning electron microscopy.

Materials and methods

Gross anatomy

The three female Eurasian lynx used in this study died from natural causes (cadaver I was 6,9 kg, cadaver II was 7,6 and cadaver III was 7,2 kg in weight, respectively). The animals were obtained from the Republic of Turkey Ministry of Agriculture and Forestry (Sivas branch) and were immediately transported to the Anatomy Department of the Veterinary Faculty of Sivas Cumhuriyet University (16). Then, we bilaterally inserted a plastic cannula into their common carotid artery and cleaned the arterial system of each cadaver with hydrogen peroxide and water solution. We fixed the cadavers with a 10% formalin solution administered via the plastic cannula. The planum nasale of each cadaver was photographed with a Canon EOS 50D camera. The nomenclature used in this study was adopted from the Nomina Anatomica Veterinaria (17).

Light microscopy

The tissue samples were fixed in buffered formalin for 24 hr, dehydrated in graded alcohol, and embedded in paraplast to create blocks. Serial sections were cut at 5–6 µm thickness. The sections were stained with a modified version of Mallory's triple stain for general histological examination (18).

Scanning electron microscopy

The specimens collected from the planum nasale samples were washed in distilled water and 2.5% glutaraldehyde three times (10 min each), dehydrated in an ascending series of ethyl alcohol solutions (50%, 70%, 90%, and 100% alcohol), dried until they reached the critical point using liquid carbon dioxide, and mounted on metal stubs. The samples were coated with a gold-palladium alloy using a sputtering device; then, we examined and photographed the specimens with a scanning electron microscope (Zeiss, Germany) (10kV) at the Advanced Technology Research Centre of Sivas Cumhuriyet University, Sivas (19).

Ethical Statement: This study was approved by the Republic of Turkey Ministry of Agriculture and Forestry (Sivas branch) (09.08.2018-72784983-488.04-176382).

Results

Gross morphology

The planum nasale of the Eurasian lynx is located around the two nostrils and the middle area of the upper lip. Its skin surface is hairless, glabrous, moist, and grayish-black, and it has a dermatoglyphic pattern consisting of epidermal ridges (see Figure 1). It was divided by a philtrum into two equal halves, around the nostril and only the middle area of the upper lip (see Figure 1). The planum nasale of Eurasian lynx was in the form of a sketchy ship anchor shape consisting of arm, palm, shank, stock, and shackle parts (see Figure 1A). The arm of the ship anchor was directed to the dorsum nasi, while the shank was directed toward the ventral of the planum nasale. The arm of the planum nasale (the arrow in Figure 1A) is located dorsally to the tip of the nose, while its palm ("Pa" in Figure 1A) is situated at the dorsolateral wings of the nose, directed medioventrally. A black dorsal border (the arrow in Figure 1A) was evident between the hairy skin of the dorsum nasi and the arm of the planum nasale. The dorsal border of the planum nasale's arm was concavely directed toward the dorsum nasi. The width of the planum nasale arm dorsally supported the nostril ("Ns" in Figure 1A) and was wider than the planum nasale's palm. The planum nasale's palm ("Pa" in Figure 1A) on both sides situated the lateral wings of the nose and the dorsolateral of the planum nasale. The width of the planum nasale's arm dorsally surrounding the nostril was wider than the planum nasale's

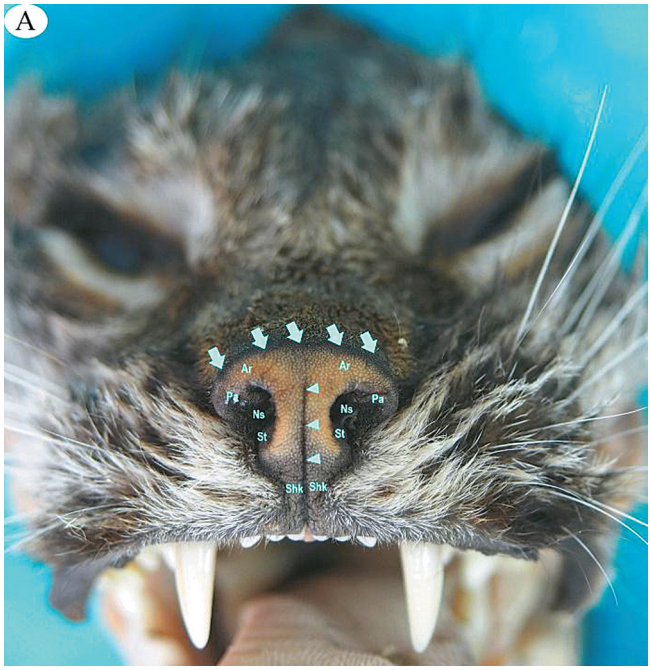

Figure 1A: The macroscopic view of Eurasian lynx Planum nasale. (A) A photograph of the planum nasale's anatomical structures: the arm (Ar), palm (Pa), and dorsal border of the planum nasale (arrow); the nostril (Ns); the philtrum (arrowhead); the shank (Sh); and the shackle (Shk) and stock of the planum nasale (St)

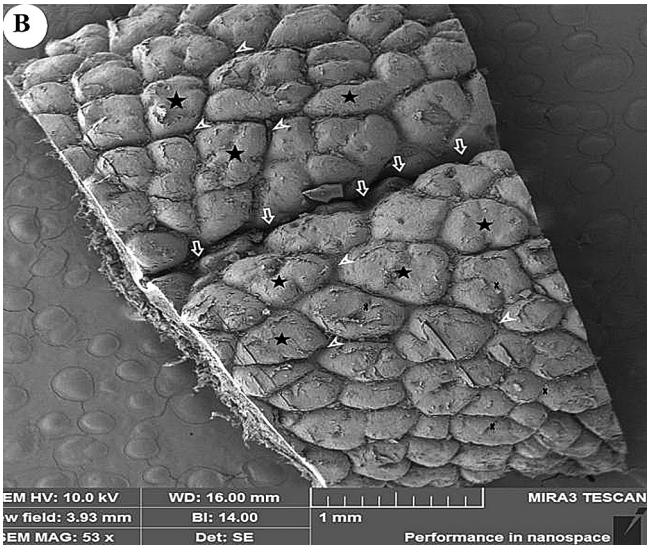

Figure 1B: An SEM image of a planum nasale's surface, with the epidermal ridges (stars), shallow fissures (arrowhead), secondary fissures (the mark), and small pores (stars).

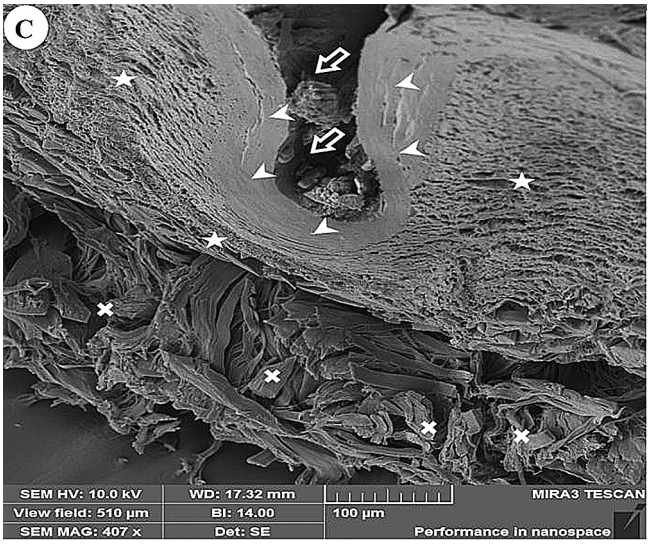

Figure 1C: An SEM image of a planum nasale's surface and section, with a profound groove (arrows), the epidermis (arrowheads), the dermis (star), and connective bundles (X mark)

palm. The planum nasale palm on either side was situated around the lateral wings of the nose and dorsolateral limited the nostrils. The lateral border of the convex planum nasale palm firstly began from the dorsal side of the nostril, then continued to the medial side, and finally ended at the ventral side. The lateral and dorsal borders of the planum nasale and philtrum (arrowhead in Figure 1A) were dark-colored glabrous skin, unlike the arm, which comprises glabrous light-colored skin in the central portion planum nasale's arm. The planum nasale's shank ("Sh" in Figure 1A) is situated in the area between the left and right nostrils. The philtrum (the arrowhead in Figure 1A) extended from the dorsal midline of the planum nasale's shank to the planum nasale's shackle and upper lip. The planum nasale's stock ("St" in Figure 1A) is located mediolaterally in the ventral portion of the planum nasale, and the ventral part of the planum nasale shank narrows dorsally to the upper lip to become the shackle of the planum nasale ("Shk" in Figure 1A). The skin of the planum nasale's shackle and the upper lip was dark and is divided into two equal halves by the philtrum. The glabrous skin surfaces of the planum nasale have many moist dermal protuberances and grooves (the star in Figure 1A), which were wider and darker in the central area of the planum nasale than at the edges of the planum nasale.

Histological Examination: The glabrous skin of planum nasale in the Eurasian lynx histologically consisted of the epidermis (Figure 2A) and dermis (Figure 2A) layers. Deep indentations (Dermal papillae) were seen (Figure 2B) between the epidermis and dermal layers. The epidermis, formed by the hairless keratinized squamous

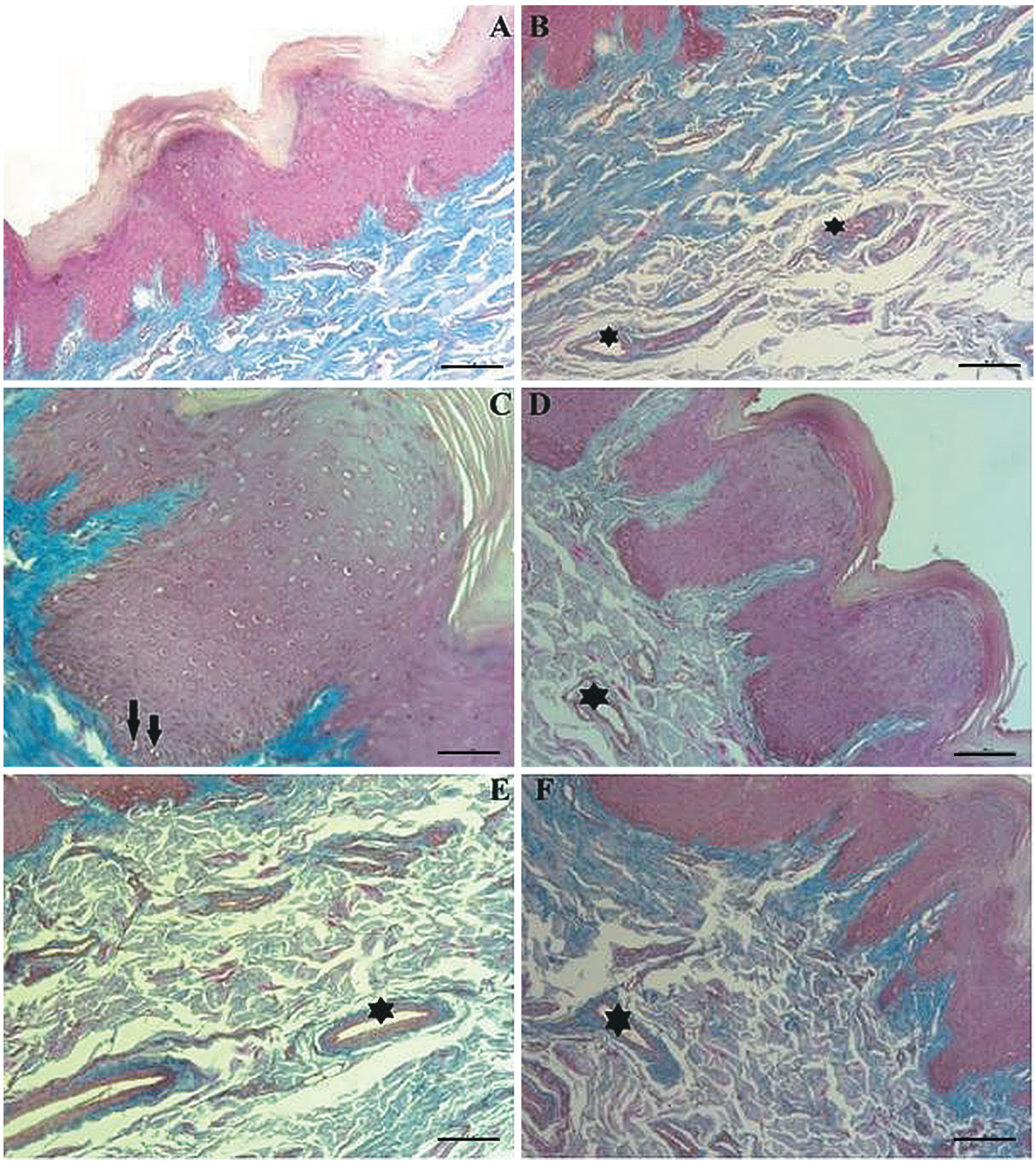

Figure 2: The histological view of Eurasian lynx planum nasale

epithelium, was composed of the basal, spinous, granular, lucid, and corneum strata in the histological preparations stained with triple stain. In the samples, the basal stratum was formed by single layers of cells located on the basement membrane (arrow in Figure 2C). The mechanoreceptor cells were seen in the basal layer. These cells were thought to have endings in the immediate vicinity (in Figure 2C). The granular layer was composed of two to three cell rows, while the spinous layer consisted of three to five polyhedral cell rows (mark in Figure 2C). The stratum corneum was the most superficial on the epidermis; it is thin and has multiple layers of ceratinocytes. The boundaries of the dermis layer, which has deep and superficial layers, were not evident in the triple-stained preparations. Deep in the dermis were more connective fibers than in the superficial areas. In addition, abundant veins and venules were situated (star in Figure 2D–F) in the dermis layer.

Scanning electron microscopy examination

The SEM surface examination showed many differently sized epidermal ridges in the samples (the stars in Figure 1B), separated from one another by shallow fissures (the arrowheads in Figure 1B). The epidermal ridges were divided into more small domes by secondary fissures (the mark in Figure 1B). The shapes of the epidermal ridges differ from each other, both among samples and between the halves of the same animal specimens. Small pores were situated in the middle of the epidermal ridges (the plus in Figure 1B). The philtrum was a profound groove in the middle line of the samples (the arrows in Figure 1B). The SEM depth module examination of the samples showed that both the philtrum and skin epidermal ridges were composed of epidermal layers (the arrowheads in Figure 1C) and that the dermal layers included dense connective bundles with different sizes and directions (the star and X mark in Figure 1C).

Discussion

The unique anatomical structures of the skin, such as the planum nasale, form through skin differentiation in various regions. The region, as previously described in ruminants (5, 7) and lemurs (3), is an extensive and easily distinguishable patch of moist, glabrous skin around the nostrils in the Eurasian lynx. In addition, the species' planum nasale has a dark border on the dorsal, lateral, and ventral sides.

On close macroscopic inspection, the planum nasale surface of the Eurasian lynx appears to be composed of packed polygonal plates or epidermal ridges, fissures, and a philtrum, as depicted in carnivores (8, 9), camels (5), and lemurs (3). In addition, the shape of the Eurasian lynx's planum nasale resembles a ship anchor consisting of arm, palm, shank, stock, and shackle parts. The arm and palm are situated dorsally to the nostrils, while the shank and stock parts are located medially and ventrally, respectively, to the nostrils in the Euroasian lynx. As previously described in ruminants (5, 6, 7, 20) and lemurs (3), the philtrum also divides the planum nasale into two halves in the Eurasian lynx. Moreover, as shown by the gross and SEM samples, in the Eurasian lynx, it has been seen that the philtrum continues to the middle of the upper lip and divides the upper lip.

In the macroscopic and SEM examinations, we found that the shapes of the epidermal ridges differ between the planum nasale halves from the same individual and among the planum nasale of different individuals. The findings are similar to descriptions reported of primates by Clifford and Witmer (12) and of cattle by Solis and Maala (14). As described by literature (12, 14), the different shapes of the planum nasale's skin plates may be used for individual identification of the animals as nose prints. In addition, we observed that the pores are situated on some skin plates. The skin plate is split into multiple secondary skin plates with shallow grooves. We observed that the shapes of the skin plates differed from of camels those photographed with SEM microscopy (5).

In agreement with findings from the literature (3, 5), we observed that the histological structure of the planum nasale's skin consisted of the epidermis and dermal layers. However, the hypodermal layer could not be seen in this study. As reported in the literature (3, 5), a wavy border was seen between the epidermis and dermal layers because of the evident epidermis and dermal papillae in the histological samples. In this study, we saw that the basal sheet of the epidermal layer was formed by a single cell layer, as depicted in *Lemur catta* (3) and camels (5), whereas our findings of Mercel's cells in the sheets were only similar to the description by Elofsson et al. (3) in *Lemur catta*. In addition, as reported by previous studies (3, 5), we observed that the granular sheet was thinner than the spinous sheet. The superficial stratum corneum of the planum nasale in the Eurasian lynx is the same as that of camels (5) and *Lemur catta* (3), in terms of thickness.

Our findings, such as dense connective fibers, rich blood vessels, and dermal papillae in the dermal layers, resemble the statements by Eshrah (5) in camels and Elofsson *et al.* (3) in *Lemur catta*.

Conclusion

The nasal plane or planum nasale of the Eurasian lynx was investigated. In this study, we observed that the Eurasian lynx's planum nasale consists of glabrous, moist, and hairless skin around nostrils and that its gross morphological shape is in the shape of a ship anchor consisting

of arm, palm, shank, stock, and shackle parts. Both the morphological and SEM investigations show that the planum nasale's skin is divided by primary and secondary fissures and splinted into epidermal ridges with different sizes and shapes. The different surface shapes of the epidermal ridges in the Eurasian lynx are used for individual identification by nose print, as in other animals. In the histological examination, we saw that the planum nasale's skin is composed of dermis and epidermal layers. The unmyelinated nerve endings located on the basal sheet of the epidermal layers may be evidence of a sensitive structure. In the SEM examination, we saw small pores on the epidermal ridges and dense bundles in the dermal layers. The dense bundles may create resistance against mechanical effects.

Acknowledgments

We would like to thank the Republic of Turkey Ministry of Forestry (Sivas Branch) for permission to conduct studies on the Eurasian lynx (Lynx lynx).

This study was not supported by any foundation.

The authors declare that they have no conflict of interest. Statement of Animal Rights all applicable international, national, and/or institutional guidelines for the care and use of animals were followed.

References

1. Ozgel O, Aykut M. Macro anatomical investigation on ossa membri pelvini of Anatolian bobcat Lynx. Pakistan J Zool 2015; 47: 1492–4.

2. Hansen K. Bobcat: master of survival. Oxford : University Press, 2007.

3. Elofsson R, Tuminaite I, Kröger RHH. A complex sensory organ in the nose skin of the promisisian primate *Lemur catta*. J Morphol 2015; 276: 649–76. doi: 10.1002/jmor.20363

4. Elofsson R, Tuminaite I, Kröger RHH. A novel ultrastructure on cornicocyte surface of mammalian nasolabial skin. J Mammal 2016; 95: 1288–94. doi: 10.1093/jmammal/gyw112.

5. Eshrah EA. The camel rhinarium: a study revealing the presence of the nasal plane in the dromedary camel (*Camelus dromedarius*) with special reference to its epidermal structure. Anat Histol Embryol 2017; 46: 65–72. doi: 10.1111/ahe.12238

6. Maya S, Chungath JJ, Ashok N, Lucy KM, Sreeranjini AR, Indu VR. Comparative morpho-histology of muzzle in deer and goat. J Indian Vet Assoc 2015; 12: 46–9.

7. Kalita HC, Kalita PC. Comparative gross anatomical studies on the muzzle of the mithun (*Bos frontalis*), yak (*Bos grunniens*) and zebu (*Bos indicus*). Indian J Anim Res 2004; 38: 150–2.

8. Dyce KM, Sack WO, Wensing CJG. Textbook of veterinary anatomy. Saunders. 1996.

9. Getty R. Sisson and Grossman's the anatomy of the domestic animals. WB Saunders. 1975.

10. König HE, Liebich HG. Veterinary anatomy of domestic mammals: Textbook and colour atlas. Schattuer. 2004.

11. Nickel R, Schummer A, Seiferle E. The viscera of the domestic animals. Verlag Paul Parey. 1973.

12. Clifford AB, Witmer LM. Case study in novel narial anatomy: The enigmatic nose of moose (Artiodactyla: *Cervidae Alces alces*). Journal of Zoology 2004; 262: 339–60. doi: 10.1017/S0952836903004692

13. Kozma SM. Feasibility of animal nose print identification using two-dimensional image correlation [Unpublished master's dissertation]. San Diego University, 2004.

14. Solis JA, Maala CP. Muzzle printing as a method for identification of cattle and carboas. Philippine Journal of Medicine 1975; 14: 1–4

15. Arı HH, Kuru N, Uslu S, Özdemir Ö. Morphological and histological study on the foot pads of the Anatolian bobcats (*Lynx lynx*). The Anatomical Record, 2018; 301: 932–8. doi: 10.1002/ar.23761

16. Anonymous. Cumhuriyet University was delivered dead Lynx in Sivas in order to make the post-mortem examination. 2016. www.sivas.ormansu.gov.tr/sivas/Anasayfa/resimliHaber.

17. International Committee on Veterinary Gross Anatomical Nomenclature. Nomina Anatomica Veterinaria. 2012.

18. Bancroft JD. Cook HC. Manual of histological techniques. Livingstone, 1984.

19. Mahdy MAA, Abdalla KEH, Mohamed SA. Morphological study of the hard palate in the Egyptian goat (*Capra hircus*): A scanning electron microscopic study. Anatomia, Histologia, Embryologia, 2018; 47: 391–397. doi: 10.1111/ahe12366

20. Metwally MA, Huissieni HB, Kassab AA, Eshrah EA. Comparative anatomy of the nasal cavity in the buffaloes, camels and donkeys. Journal of Veterinary Medicine Research 2019; 9: 69–75.

MORFOLOGIJA IN HISTOLOGIJA SMRČKA EVRAZIJSKEGA RISA (*Lynx lynx*)

H. H. Ari, S. Uslu

Izvleček: V študiji so opisane makroskopske in mikroskopske strukture smrčka evrazijskega risa, ki je bila opravljena s proučevanjem tkiv treh mrtvih samic, ki so jih pridobili s pomočjo gozdarske podružnice Sivas Ministrstva za kmetijstvo in gozdarstvo Republike Turčije. Strukturo smrčka so raziskovali z uporabo makroskopskih, histoloških metod ter uporabe vrstičnega elektronskega mikroskopa (SEM). Mikroskopska preiskava je pokazala, da smrček sestavlja brezdlaka, vlažna, gola koža, ki po obliki spominja na ladijsko sidro. Površinski del smrčka tvorijo epidermalne plošče ali grebeni, ki jih ločujejo primarne in sekundarne razpoke, vidne na makroskopskih slikah in s pomočjo vrstične mikroskopije. Na histoloških preparatih so bile v bazalni plasti smrčka epidermisa opazne Merkelove celice in živčni končiči. S pomočjo metode SEM so v plasti epidermisa pokazali pore, ki se nahajajo na površini epidermalnih grebenov in snope togega fibrilarnega veziva, ki segajo v plast dermisa.

Ključne besede: Evrazijski ris (*Lynx rufus*); morfologija; nosna ravnina; smrček

Slov Vet Res 2021: 58 (4): 155 – 8
DOI 10.26873/SVR-1331-2021
UDC 636.7.09:616.211:616.99:595.772(497.4)

Case Report

FIRST REPORT OF CANINE MYIASIS WITH SHEEP NASAL BOT FLY, *Oestrus ovis*, IN SLOVENIA

Aleksandra Vergles Rataj*, Petra Bandelj, Vladimira Erjavec, Darja Pavlin

[1]Veterinary Faculty, University of Ljubljana, cesta V Mestni log 47, Sl-1115 Ljubljana, Slovenia

*Corresponding author, Email: aleksandra.verglesrataj@vf.uni-lj.si

Abstract: First larval stage (L1) of *Oestrus ovis* was recovered by flushing of the nasal cavity during rhinoscopy in an urban living dog. The dog was taken to the Small animal clinic after an acute onset of sneezing and bilateral nasal discharge. In Europe, there are sporadic reports of nasal myiasis in dogs caused by sheep bot flies, and the overall prevalence of *O. ovis* is high in Mediterranean countries. Because of its habitat expansion due to climate change, it should be considered as a differential diagnosis when an animal patient presents with signs of rhinitis in areas bordering the Mediterranean climate. This is the first report of a dog infested by sheep nasal bot fly in Slovenia.

Key words: *Oestrus ovis*; sheep bot fly; nasal myiasis; dog; climate change

Introduction

The sheep ectoparasite, *Oestrus ovis* L. (Linnaeus 1758) is commonly known as nasal bot fly of sheep, goats, and other wild ruminants (1), although infestations of dogs (2, 3, 4, 5, 6), humans (7) and a cat (8) have also been documented. It has a worldwide distribution, with a preference to warmer climate, where adult flies can be active year-round (9). In Europe, it has a high prevalence in Mediterranean regions, where seroprevalence in sheep can reach from 43.3-91% (10, 11, 12). In Slovenia, the prevalence was assessed at 40% (13). The presence of the parasite in the population can be detrimental to the infested animals (12, 14), as the larval stages of the *O. ovis* invade sinu-nasal passages (1). If the infestation is severe, the animal may suffer further complication of the respiratory system, such as chronic pneumonia unresponsive to antimicrobial treatment (15). Reports of dogs with *O. ovis* infestation are rare but show that dogs can harbor all stages of larvae, including mature larval instar (5). Clinical signs in dogs are mild in the early stage of infestation (4) but can become severe if symptoms go unnoticed, even leading to euthanasia of the animal (3). With some exceptions (3), most cases are associated with the dog or cat living on a sheep farm or in an area of high sheep density (4, 5, 8).

Received: 22 April 2021
Accepted for publication: 27 July 2021

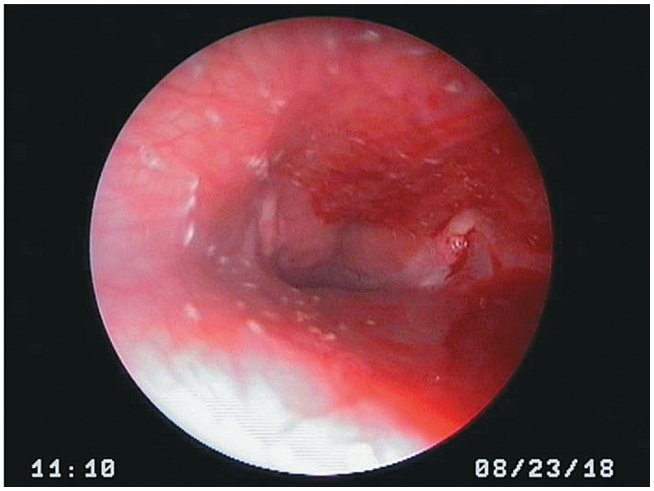

Figure 1: Multiple *Oestrus ovis* L1 in the nasopharynx of the dog during retroflex nasopharyngoscopy

Figure 2: *Oestrus ovis* L1 segmented body with two dark brown oral hooks (arrow) on the first body segment

Figure 3: *Oestrus ovis* L1 caudal spines on the last body segment

The aim of this report is to describe the first case of sheep nasal bot fly infestation in a dog in Slovenia with no history of being in contact with sheep or sheep associated areas.

Case presentation

In August 2018, a spayed 4-year-old West Highland White Terrier female dog living in the city of Ljubljana (latitude 46°03'03" N, longitude 14°30'18" E) was presented to the Small animal clinic (Veterinary Faculty, University of Ljubljana) with frequent sneezing and nose licking of an acute onset. The owner reported that the clinical signs started after the dog was taken for a walk to a nearby meadow field in the city center. Clinical examination of the dog revealed low grade serous bilateral nasal discharge with no other changes in her clinical status. A complete blood count was performed to rule out infectious diseases, which showed no abnormalities. Based on the suspected diagnosis of a nasal foreign body, a rhinoscopy was performed the same day. Mild oedema and erythema of the mucosal surface with several small moving larvae-like structures was noticed in the nasal cavity (Figure 1). More than 30 larvae-like structures were noted further down the nasopharynx. Retrograde irrigation of the nasal cavity with saline removed the larvae-like structures, which were sent to the Parasitology department of the Veterinary Faculty (University of Ljubljana) for identification. While waiting for a parasitological diagnosis, the dog was treated with ivermectin (Ivomec 1%, Merial) at a dose of 0.03 mg/kg, applied subcutaneously three times at weekly intervals. The owner stated that the clinical signs subsided within the first week of starting treatment and disappeared completely two weeks after the initial diagnosis. The sneezing resolved one day after rhinoscopy and nasal lavage.

The parasitological diagnosis of first larval stage (L1) of *Oestrus ovis* L (Diptera, Oestridae) was made, based on key morphological features (16) observed under light microscopy. The dorsoventrally flattened L1 was approximately 1.2 mm long and 0.4 mm wide. The larval body was divided into 11 segments, with a pair of prominent, dark brown oral hooks on the first segment (Figure 2) and caudal spines on the last segment (Figure 3).

Discussion

Nasal bot fly, *Oestrus ovis*, causes myasis in small ruminants (1), but other casual hosts, such as humans (7) and carnivores (2-6, 8) have also been reported. The presence of sheep nasal bot flies in Slovenia was recorded in 1997 with a seroprevalence of 40% (13). Since then, several cases have been reported in Slovenia, in which third stage larvae were identified in sheep (unpublished data). In this study, we report the first case of *O. ovis* L1 infestation in a dog in Slovenia.

The dog presented in this case, lives in the city of Ljubljana, which has a pre-alpine climate. As discussed by Zanzani et al (6), climate change may have been an important component in the spread of *O. ovis* habitat above 45° N latitude. Although there have been sporadic local reports of nasal bot fly infestation in sheep, no study has been done to determine its prevalence since 1997 (13). The 4-year-old dog lived most of its life in an urban environment. According to the owner, the dog had no contact with sheep or areas associated with sheep. However, Ljubljana as a city is still highly accessible to the rural surroundings, where flocks of sheep are present. It is common for dog owners who live in the city to walk their dogs through the livestock pastures and rural areas, especially in the summer. Adult nasal bot flies are very active during the hot summer months (14, 17) and explains the infestation of the dog in August. If the infestation would go unnoticed by the owner, the *O. ovis* L1 would remain quiescent during the cold winter months and continued its development the following spring (14, 17). This was the case of a dog in the UK, where the dog expelled the mature larva in the spring of 2011, following the presumptive infestation in autumn 2010 (5).

Reportedly the infestation of *O. ovis* in dogs and cats are less likely than in humans (6), where it usually causes ophthalmomyiasis (7, 18). To the authors knowledge, no human cases have been documented in Slovenia to date. However, there have been several cases of human ophthalmomyiasis in Italy and two recent cases in Croatia (7). It is suspected that the incidence of ocular myiasis in humans is underreported (7), as is with canine cases of nasal myiasis (6). Nasal myiasis due to *O. ovis* infestation should be considered as a differential diagnosis when an animal is presented with signs of rhinitis, sneezing and nasal discharge (3, 4, 6). With climate change the prevalence and distribution of *O. ovis* may increase and expand (5) to non-Mediterranean regions. In conclusion, it is important to emphasize the role of reporting disease occurrence in both, animals and humans, and determining the prevalence of sheep nasal bot flies in populations previously believed not to be at risk.

References

1. Zumpt F. Myiasis in man and animals in the old world: a textbook for physicians, veterinarians and zoologists. London : Butterworths, 1965.

2. Lucientes J, Ferrer-Dufol M, Andres MJ, Peribanez MA, Gracia-Salinas MJ, Castillo JA. Canine myiasis by sheep bot fly (Diptera: Oestridae). J Med Entomol 1997; 34(2): 242–3.

3. Luján L, Vázquez J, Lucientes J, Panero JA, Varea R. Nasal myiasis due to *Oestrus ovis* infestation in a dog. Vet Rec 1998; 142(11): 282–3.

4. Heath ACG, Johnston C. Nasal myiasis in a dog due to *Oestrus ovis* (Diptera: Oestridae). N Z Vet J 2001; 49(4): 164.

5. McGarry J, Penrose F, Collins C. *Oestrus ovis* infestation of a dog in the UK. J Small Anim Pract 2012; 53(3): 192–3.

6. Zanzani SA, Cozzi L, Olivieri E, Gazzonis AL, Manfred MT. *Oestrus ovis* L. (Diptera: Oestridae) induced nasal myiasis in a dog from Northern Italy. Case Rep Vet Med 2016; 2016: e5205416. doi: 10.1155/2016/5205416

7. Pupić-Bakrač A, Pupić-Bakrač J, Škara Kolega M, Beck R. Human opthalmomyiasis caused by *Oestrus ovis* – first report from Croatia and review on cases from Mediterranean countries. Parasitol Res 2020; 119(3): 783–93.

8. Webb SM, Grillo VL. Nasal myiasis in a cat caused by larvae of the nasal bot fly, *Oestrus ovis*. Aust Vet J 2010; 88(11): 455–7.

9. Sotiraki S, Hall MJR. A review of comparative aspects of myiasis in goats and sheep in Europe. Small Ruminant Res 2012; 103(1): 75–83.

10. Dorchies P, Bergueaud JP, Tabouret G, Prevot F, Jacquiet P. Prevalence and larval burden of *Oestrus ovis* (Linné, 1761) in sheep and goat in northern Mediterranean region of France. Vet Parasitol 2000; 88(3/4): 269–73.

11. Scala A, Solinas G, Citterio CV, Kramer H, Genchi C. Sheep oestrosis (*Oestrus ovis*, Linné

1761, Diptera, Oestridae) in Sardinia, Italy. Vet Parasitol 2001; 102(1/2): 133–41.

12. Alcaide M, Reina D, Sánchez-López J, Frontera E, Navarrete I. Seroprevalence of *Oestrus ovis* (Diptera, Oestridae) infestation and associated risk factors in ovine livestock from Southwestern Spain. J Med Entomol 2005; 42(3): 327–31.

13. Brglez J, Polajner V. Oestrosis in sheep. Vet Nov 1997; 23: 393–4.

14. Hall M, Wall R. Myiasis of humans and domestic animals. Adv Parasitol 1995; 35: 257–334.

15. Gomez-Puerta LA, Alroy KA, Ticona DS, Lopez-Urbina MT, Gonzalez AE. A case of nasal myiasis due to *Oestrus ovis* (Diptera: Oestridae) in a llama (*Lama glama*). Rev Bras Parasitol Vet 2013; 22(4): 608–10.

16. Colwell DD. Larval morphology. In: Colwell DD, Hall MJ, Sholl PJ, eds. The Oestrid flies: biology, host-parasite relationship, impact and management. Cambridge : CABI Publishing, 2006: 98–122.

17. Cepeda-Palacios R, Angulo Valadez CE, Scholl JP, Ramirez-Orduna R, Jacquiet P, Dorchies P. Ecobiology of the sheep nose bot fly (*Oestrus ovis* L.): a review. Revue Méd Vét 2011; 162(11): 503–7.

18. D'Assumpcao C, Bugas A, Heidari A, Sofinski S, McPheeters RA. A case and review of ophthalmonyiasis caused by Oestrus ovis in the central valley of California, United States. J Investig Med High Impact Case Rep 2019; 7: e2324709619835852. doi: 10.1177/2324709619835852

PRVI PRIMER PASJE MIAZE Z OVČJIM NOSNIM ZOLJEM, *Oestrus ovis*, V SLOVENIJI

A. Vergles Rataj, P. Bandelj, V. Erjavec, D. Pavlin

Izvleček: Med rinoskopijo in spiranjem nosne votline, smo pri psu, ki živi v urbanem okolju, ugotovili ličinke prve stopnje (L1) zajedavca *Oestru ovis*. Lastniki so psa pripeljali na Kliniko za male živali po akutnem izbruhu kihanja in bilateralnega nosnega izcedka. V Evropi so dokumentirani sporadični primeri nosne miaze pri psih zaradi ovčjega nosnega zolja, *O. ovis*, in skupna prevalenca ovčjega zajedavca je v mediteranskih državah visoka. Zaradi klimatskih sprememb, se habitat nosnih zoljev čedalje bolj širi, za kar je pomembno *O. ovis* vključiti v seznam diferencialnih diagnoz pri pacientih s kliničnimi znaki rinitisa tudi na področjih, ki mejijo na mediteransko klimo. To je prvi opisan primer infestacije psa z ovčjim nosnim zoljem v Sloveniji.

Ključne besede: *Oestrus ovis*; ovčji nosni zolj; nosna miaza; pes; podnebne spremembe

AUTHOR INDEX VOLUME 58, 2021

SLOVENIAN VETERINARY RESEARCH
SLOVENSKI VETERINARSKI ZBORNIK

Slov Vet Res 2021; 58 (4)

Original Research Articles

Case Report